学位論文

X-ray crystallography of mutant actins which affect calcium regulation of muscle contraction

（筋収縮制御に影響を及ぼす変異アクチンの
X線結晶構造解析）

平成１１年１２月博士（理学）申請

東京大学大学院理学系研究科
物理学専攻
松浦能行

X-ray crystallography of mutant actins which affect calcium regulation of muscle contraction

Yoshiyuki Matsuura

Department of Physics, School of Science, University of Tokyo, Hongo 7-3-1, Bunkyo-ku, Tokyo 113-0033, Japan

submitted to University of Tokyo as a partial fulfillment of the requirements for the Degree of Doctor of Science

December, 1999

Contents

Summary

Replacement of residues 228-230 or 228-232 of subdomain 4 in *Dictyostelium* actin with the corresponding *Tetrahymena* sequence (QTA to KAY replacement: half chimera-1; QTAAS to KAYKE replacement: full chimera) leads to a higher Ca^{2+}-activation of the regulated acto-myosin subfragment-1 ATPase activity. The ratio of ATPase activation in the presence of tropomyosin-troponin and Ca^{2+} to that without tropomyosin-troponin becomes about four times as large as the ratio for the wild-type actin. To understand the structural basis of this higher Ca^{2+}-activation, we have determined the crystal structures of the 1:1 complex of *Dictyostelium* mutant actins (half chimera-1 and full chimera) with gelsolin segment-1 to 2.0 Å and 2.4 Å resolution, respectively, together with the structure of wild-type actin as a control. Although there were local changes on the surface of the subdomain 4 and the phenolic side chain of Tyr230 displaced the side chain of Leu236 from a nonpolar pocket to a more solvent-accessible position, the structures of the actin chimeras showed that the mutations in the 228-232 region did not introduce large changes in the overall actin structure. This suggests that residues near position 230 formed part of the tropomyosin binding site on actin in actively contracting muscle. The higher Ca^{2+}-activation observed with A230Y-containing mutants can be understood in terms of a three-state model for thin filament regulation (McKillop, D.F.A. & Geeves, M.A. (1993). *Biophys. J.* **65**, 693-701) in which, in the presence of both Ca^{2+} and myosin heads, the local changes of actin generated by the mutation (especially its phenolic side chain) facilitate the transition of thin filaments from a "closed" state to an "open" state. Between 394 and 469 water molecules were identified in the different structures and it was found that actin recognizes hydrated forms of the adenine base and the Ca^{2+} ion in the nucleotide binding site.

Abbreviations used: S1, myosin subfragment-1; G1, gelsolin segment-1; EGTA, ethyleneglycol-bis-(β-aminoethyl ether) *N,N,N',N'*-tetraacetic acid; MES, 2-(*N*-morpholino) ethanesulfonic acid; r.m.s., root-mean-square.

1. Introduction

1.1 Muscle contraction and its regulation by Ca^{2+}

Muscle contraction is generated by thick (myosin-containing) and thin (actin-containing) filaments sliding past each other (Figure 1; Huxley & Neidergerke, 1954; Huxley & Hanson, 1954). In skeletal and cardiac muscle, contraction is regulated by the level of intracellular Ca^{2+} and is mediated at the level of thin filaments which consist of troponin, tropomyosin and actin (Ebashi & Endo, 1968). In relaxed muscle, the concentration of Ca^{2+} in the cytosol is maintained below 1 μM and the actin-myosin interaction is inhibited by the troponin-tropomyosin system. When the cytosolic Ca^{2+} concentration increases to about 10 μM, Ca^{2+} binds to troponin and triggers series of conformational changes in thin filaments that ultimately lead to an active cyclic interaction between actin and myosin driven by the hydrolysis of ATP.

The unit of a cross-striated muscle is the sarcomere (Figure 1). The boundaries of the sarcomere are the Z-lines. Between the Z-lines, lie the bipolar thick filaments composed substantially of the protein myosin. Each myosin molecule is comprised of a long double α-helical tail portion and two globular heads. The tails aggregate to form the thick filaments. The two flexibly attached globular heads are variously known as the heads, the myosin subfragment 1 (S1) portions, or the cross-bridges. The heads, which may be prepared by mild proteolytic cleavage, retain the ability to hydrolyze ATP and to interact with actin. To avoid the problems associated with aggregation of myosin, solution biochemical studies are often done using the S1 fragments.

In the sarcomere, thin filaments are joined onto each side of the Z-line. Thin filaments are based on a helical arrangement of actin (F-actin) which can be thought of as two strands of globular actin monomers (G-actin) twisted round one another. The crystal structure of G-actin in complex with either DNase I, gelsolin segment 1 or profilin has

been established (Figure 2; Kabsch *et al.*, 1990; Schutt *et al.*, 1993; McLaughlin *et al.*, 1993; Chik *et al.*, 1996) and has been used to infer the atomic structure of F-actin filaments (Figure 3; Holmes *et al.*, 1990; Lorenz *et al.*, 1993). Tropomyosin is a rod-shaped coiled-coil protein (Whitby *et al.*, 1992) that lies in the grooves of F-actin spanning seven G-actins. Troponin, a complex of three chains, binds to both tropomyosin and actin. Conformational changes in troponin induced by changes in the Ca^{2+} concentration are transmitted to thin filaments and modulate the interaction between actin and the S1 heads of myosin and so control muscle contraction.

The docking of myosin heads to actin is fundamentally important in muscle contraction and is known to be a multi-step process. Kinetically the docking of myosin onto an actin filament can be resolved into at least two events (Geeves, 1991; see Figure 4A). Geeves and his colleagues proposed that all myosin and myosin-nucleotide complexes bind to actin in the same pathway, via two major events, but the nature of the bound nucleotide has a major influence on the equilibrium constant of the last step shown schematically in Figure 4A. In the A-state, myosin-actin affinity is low and so this state is often referred to as the weak-binding state. The formation of the A-state is relatively independent of the nucleotide bound to myosin. The transition from A-state to R-state results in a major strengthening of the actin binding to myosin and simultaneously a weakening of the nucleotide-binging to myosin. The equilibrium constant of this step varies for different nucleotides. Thus, in the absence of nucleotide, K_2 is large (>100), in the presence of ATP it is small ($K_2 << 1$), and ATP displaces actin. For other nucleotides and nucleotide analogs, K_2 is intermediate. The essential proposals of this model are that the docking process is an inherent property of the acto-S1 proteins, that the role of ATP binding and hydrolysis is to allow this docking to be repeated, and that the last event in the docking (the A-to-R isomerization) is coupled to the fast product release from myosin active site (and so acceleration of myosin S1 ATPase) and the force generating event in muscle contraction.

Since it was originally proposed in 1970s, the most attractive working hypothesis in calcium regulation has been the steric blocking theory, in which the position of tropomyosin on actin filaments is considered to be critical in the control of actin-myosin interaction (Haselgrove, 1972; Huxley, 1972; Parry & Squire, 1973; Wakabayashi *et al.*, 1975). Thus, in the "off" state (in which contraction is prevented) tropomyosin is proposed to be located at a high radius where it obstructs the binding site for the myosin S1 heads on actin, whereas in the "on" state (corresponding to muscle contraction) tropomyosin is proposed to move to a lower radius, deep in the actin groove, unmasking the S1 binding site. More recent work has indicated that the simple steric blocking mechanism may be an oversimplification and there are indications that not only tropomyosin movement but also other factors such as troponin movement and actin conformational changes are involved in calcium regulation (for a review, see Squire & Morris, 1998). However, at least in skeletal muscle, the movement of tropomyosin in the actin groove between "on" and "off" states appears to be well established (Lehman *et al.*, 1994; Ishikawa & Wakabayashi, 1994; Lehman *et al.*, 1995; Vibert *et al.*, 1997; Ishikawa & Wakabayashi, 1999) although the precise manner in which this movement regulates contraction is still controversial (reviewed by Squire & Morris, 1998). The precise location of tropomyosin in the "off" state needs to be determined carefully, because it has been assumed that the density due to troponin would not contribute to the three-dimensional images reconstructed by imposing helical symmetry and that tropomyosin follows the actin symmetry but these assumptions may be less valid in the "off" state than in the "on" state. Moreover, careful kinetic measurements (McKillop & Geeves, 1993) have indicated that a three-state model for regulation is more appropriate (Figure 4B; see also Table 1), in which tropomyosin occupies a "blocked" state (where steric blocking prevents the binding of S1), a "closed" state (where S1 can only bind in its weak state configuration) and an "open" state (the "on" state where S1 can bind strongly). In the absence of calcium the blocked state predominates with ~80 % of the actins in the filament in this form (20 % closed, <5 % open). In the presence of calcium but the absence of myosin heads the closed state predominates (<5 % blocked, 80 % closed, 20 %

open). This is also the preferred state of troponin-free thin filaments. The transition from the closed state to the open state is induced by strongly bound myosin heads. Thus, the full activation of thin filaments requires not only calcium but also myosin heads.

1.2 Mutational analyses of actin function

Electron microscopy has indicated the general areas of actin likely to interact with tropomyosin in the different regulatory states of thin filaments and, for example, three-dimensional electron cryo-microscopy has shown that the addition of Ca^{2+}significantly increases the density on inner domain (subdomains 3 and 4) of actin in thin filaments (Ishikawa & Wakabayashi, 1994). However, information on the precise residues involved in the interaction between tropomyosin and actin has been difficult to obtain. One clue to the actin residues involved in the "on" or "open" state has come from the behaviour of *Dictyostelium/Tetrahymena* chimeric actin, which, when complexed with tropomyosin-troponin, shows an increased activation by Ca^{2+} compared with rabbit or *Dictyostelium* actins (Saeki *et al.*, 1996; Saeki & Wakabayashi, 2000). To identify the residues responsible for this increased activation using site-directed mutagenesis, an expression system based on *Dictyostelium* was used (Figure 5; Sutoh *et al.*, 1991; Johara *et al.*, 1993; Saeki *et al.*, 1996) since actin cannot be expressed in bacteria. *Dictyostelium* actin has 91 % sequence identity with rabbit skeletal actin (Sheterline *et al.*, 1996) and *in vitro* experiments have demonstrated that the properties of *Dictyostelium* actin are very similar to those of skeletal muscle actin. *Dictyostelium* actin activates skeletal muscle myosin ATPase and shows normal calcium regulation when combined with skeletal tropomyosin and troponin (Saeki *et al.*, 1996). Therefore, *Dictyostelium* actin can be used as a substitute for skeletal muscle actin to explore the mechanism by which muscle contraction is regulated. A number of *Dictyostelium/Tetrahymena* chimeras constructed in this way have indicated that the increased activation seen with *Dictyostelium/Tetrahymena* chimeric actin derives primarily from residues 228-232 (Figure 6; Saeki *et al.*, 1996; Saeki & Wakabayashi, 2000). Thus, the "full" chimera

(originally referred to as mutant 646), in which five consecutive residues from Gln228 to Ser232 in *Dictyostelium* actin (QTAAS) are replaced by those found in *Tetrahymena* (KAYKE), shows a remarkably higher Ca^{2+}-activation when bound to tropomyosin-troponin (Saeki *et al.*, 1996). In the absence of Ca^{2+}, the full chimera shows the same low troponin-tropomyosin-acto-S1 ATPase activity observed with wild-type *Dictyostelium* actin. In the presence of Ca^{2+}, however, the full chimera activates troponin-tropomyosin-acto-S1 ATPase activity two to five times more than that of *Dictyostelium* wild-type actin (Saeki *et al.*, 1996). However, the structural basis for this higher Ca^{2+}-activation was not immediately clear from the existing knowledge of the structure of actin and other components of thin filaments and it was uncertain whether these residues were involved directly in the interaction with tropomyosin or instead generated a more global structural change in actin subdomain 4 that altered either the interaction with tropomyosin or with myosin S1.

We have now used X-ray crystallography to investigate the structural basis of this higher Ca^{2+}-activation and describe here the crystal structure of complexes of gelsolin segment 1 (G1) complexed with native *Dictyostelium* actin, the full chimera (residues 228-232 replaced by KAYKE) and a half chimera (with residues 228-230 replaced by KAY) which also shows higher Ca^{2+}-activation (Figure 6). The G1 system was used because the G1 binding site is far away from the mutation sites in subdomain 4 and also because the mutation sites are not crystal contact sites in the G1 system and so the actin-G1 complex structures were expected to reveal the mutational effects on actin structure without artifacts. Comparing these structures shows that the mutations at positions 228-232 (QTAAK -> KAYKE) or positions 228-230 (QTA -> KAY) do not change the main-chain conformation of actin. However, the side chain of Tyr230 of these mutants displaces the side chain of Leu236 from a hydrophobic pocket into a position more exposed to solvent. The effect of the mutations therefore is to generate only a local conformational change at this position on the surface of actin, indicating that they are involved directly in producing the higher Ca^{2+}-activation. This suggests that the

surface of actin subdomain 4 exerts an important influence on the transition from an "off" state towards an "on" state in the presence of both Ca^{2+} and myosin heads. In addition to the structural information related to higher Ca^{2+}-activation, the resolution obtained with the *Dictyostelium* structures (especially that of half chimera-1) was somewhat higher than had been obtained previously for actin complexes (Kabsch *et al.*, 1990; McLaughlin *et al.*, 1993; Schutt *et al.*, 1993; Chik *et al.*, 1996) and enabled a much larger number of bound water molecules to be identified. Hydration of the adenine base and Ca^{2+} ion in the nucleotide binding pocket was observed and provided insight into the more precise mode of binding of ATP and Ca^{2+} to actin. Moreover, we did not observe any water molecules located near enough to attack γ-phosphorus, which may account for the very low intrinsic ATPase activity of Ca^{2+}-G-actin (Estes *et al.*, 1992).

This work is published (Matsuura *et al.*, 2000).

2. Materials and Methods

2.1 Expression and purification of proteins

Human cytoplasmic gelsolin segment 1 with the N35C point mutation (G1) was expressed in the *E.coli* host strain BL21(DE3) and purified as described by Mannherz *et al.* (1992) with slight modifications. The soluble fraction was applied to a DEAE-Sephacel column (2.5 cm x 16 cm) in 10 mM Tris-HCl (pH 8.0), 1 mM EGTA and 1 mM DTT and protein eluted with a linear salt gradient (0 to 100 mM NaCl). Fractions containing G1 were collected, concentrated to 40 mg/ml by ultra filtration (Centriprep-3) and further purified by gel filtration over a Superdex 75 column (2.6 cm x 60 cm) equilibrated with 10 mM Tris-HCl (pH 8.0), 0.1 mM $CaCl_2$, 1 mM NaN_3, 150 mM NaCl and 1 mM DTT. Peak fractions were pooled and concentrated to 28 mg/ml by Centriprep-3.

Dictyostelium has at least 17 actin genes (Romans & Firtel, 1985), although actin 15 is by far the most abundantly expressed and is referred to as wild-type in this paper. To facilitate isolation of mutant actins, we introduced an additional mutation (E360H) which previous work has shown does not alter any of the properties of actin (Saeki *et al.*, 1996). Wild-type *Dictyostelium* actin was extracted from strain Ax2 whereas mutant actins were extracted from transformed *Dictyostelium* cells as described (Saeki *et al.*, 1996); all actins were initially purified as described (Sutoh *et al.*, 1991). Actin fractions of DEAE-5PW were further purified by two cycles of polymerization-depolymerization and the resultant G-actin solution was applied to a Superdex 75 column (2.6 cm x 60 cm) equilibrated with 2 mM Tris-HCl (pH 8.5), 0.2 mM ATP, 0.1 mM $CaCl_2$, 0.5 mM NaN_3 and 0.1 mM DTT. G-actin (most probably with bound Ca^{2+}ATP) was eluted with the same buffer and peak fractions were pooled and concentrated using Centriprep-10 to 5 mg/ml. Typical yields from 4 litre cultures were 9 mg for wild-type and 4 mg for mutants.

To produce the 1:1 complex of G1 and *Dictyostelium* wild-type actin or mutant actins, the purified G-actin and G1 were mixed in the molar ratio of 1 to 3. The mixture was incubated overnight on ice and then applied to a Superdex 75 column (2.6 cm x 60 cm) equilibrated with 10 mM imidazole-HCl (pH 7.0), 150 mM NaCl, 0.1 mM ATP, 0.1 mM $CaCl_2$, 0.1 mM $MgCl_2$, 1 mM NaN_3, and 0.1 mM DTT (buffer F) and eluted with the same buffer. The peak fractions of actin-G1 complex were pooled, concentrated to 10-20 mg/ml using Centriprep-10 and stored on ice. The protein sample was used for crystallization within a week.

2.2 Crystallization and X-ray data collection

Crystals of *Dictyostelium* wild-type actin-G1 complex were grown by vapour diffusion in hanging drops. Equal volumes of protein (5 mg/ml in buffer F) and reservoir solution (50 mM imidazole-HCl (pH 6.6), 150 mM NaCl, 0.1 mM ATP, 0.1 mM $CaCl_2$, 0.1 mM $MgCl_2$, 1 mM NaN_3, 10 mM DTT and 9 % PEG 6000) were mixed, and equilibrated at room temperature. Single crystal plates grew to a maximum size of 600 µm x 400 µm x 20 µm in one week. Immediately before data collection, the wild-type crystal was soaked in a cryoprotectant solution containing 50 mM imidazole-HCl (pH 6.6), 150 mM NaCl, 0.1 mM $CaCl_2$, 0.1 mM $MgCl_2$, 9 % PEG 6000 and 25 % glycerol for several seconds, scooped with a nylon loop and then flash-frozen in a stream of dry nitrogen gas at 100 K. Crystals of the half chimera-1-G1 complex were grown under identical conditions as used for wild-type except that 50 mM MES-NaOH (pH 6.0) was included in the reservoir instead of 50 mM imidazole-HCl (pH 6.6). Plate crystals appeared within a day after crystallization setup and grew to a maximum size of 1 mm x 400 µm x 50 µm in a few days. Prior to data collection, the crystal was dialyzed overnight against a cryoprotectant mother liquor (50 mM MES-NaOH (pH 6.0), 150 mM NaCl, 0.1 mM ATP, 0.1 mM $CaCl_2$, 0.1 mM $MgCl_2$, 1 mM NaN_3, 10 mM DTT, 20 % PEG 6000 and 30 % glycerol) using a microdialysis button. After the dialysis, the crystal was scooped with a nylon loop and flash frozen in a dry nitrogen gas stream at 100 K.

Crystals of the full chimera-G1 complex were grown under the same conditions used for half chimera-1 crystallization. Plate crystals grew to a typical size of 1 mm x 500 μm x 70 μm in two to three days. Prior to data collection, the crystals were adapted to a cryosolvent containing 20 % PEG 6000 and 30 % glycerol with successive 20-min soaks in incremental six steps of increasing PEG 6000 and glycerol concentration. Crystals were then scooped with a nylon loop and flash frozen by plunging into liquid nitrogen.

A 2.4 Å resolution data set of the wild-type complex was collected on beamline 9.6 at the Daresbury synchrotron radiation source (UK) using a MAR Research imaging plate scanner and 0.88 Å wavelength radiation. A 2.0 Å data set of half chimera-1 was obtained on beamline BL41XU (Kamiya *et al.*, 1995) at the SPring-8 synchrotron facility (Japan) using a RIGAKU imaging plate detector (R-AXIS IV) and 0.708 Å wavelength radiation. Diffraction spots were observed up to 1.7 Å resolution. A 2.4 Å resolution data set of full chimera was collected in oscillation mode on beamline BL6B at the Photon Factory synchrotron (Japan) using 1.0 Å wavelength radiation and imaging plate detector (800 x 400 mm). Data processing was performed using either the MOSFLM package (CCP4, 1994) or the HKL package (Otwinowski & Minor, 1997). The data collection statistics are summarized in Table 1. Both wild-type and mutant crystals were isomorphous with rabbit actin-G1 co-crystal (McLaughlin *et al.*, 1993).

2.3 Structure determination and refinement

The structure of *Dictyostelium* wild-type actin-G1 complex was solved by molecular replacement using AmoRe (CCP4, 1994) starting from the atomic coordinates of rabbit skeletal actin-G1 complex (McLaughlin *et al.*, 1993) which were kindly provided by Mr. Brian Pope (MRC Laboratory of Molecular Biology, Cambridge). All the mutations corresponding to *Dictyostelium* actin 15 were clear and the appropriate side-chain conformations were easily built into the $2Fo–Fc$ density. The wild-type model was then used as a model to solve the half chimera-1-G1 complex by molecular

replacement. Then the half chimera-1 model was used to solve the full chimera structure. Prior to structure determination 5 % of the data were randomly chosen and omitted for the calculation of a free *R* value (Brünger, 1992). Rigid body refinement using REFMAC (CCP4, 1994) and subsequent repeated cycles of model building by O (Jones *et al.*, 1991) and refinement by REFMAC resulted in atomic models with excellent geometry. We checked each water molecule individually and only accepted them if its inclusion decreased the free *R* factor thereby ensuring that the most reliable water molecules were included in the final model. The refinement statistics are summarized in Table 2. Atomic coordinates of wild-type, half chimera-1 and full chimera have been deposited in the Protein Data Bank with accession codes 1C0F, 1C0G and 1DEJ, respectively. The molecular graphics figures in this thesis were prepared with MOLSCRIPT (Kraulis, 1991) and Raster3D (Merritt & Bacon, 1997).

3. Results

3.1 Crystallization and X-ray data collection

To investigate the structural basis of the higher Ca^{2+}-activation of the regulated acto-myosin S1 ATPase observed in *Dictyostelium/Tetrahymena* actin chimeras (Saeki *et al.*, 1996; Saeki & Wakabayashi, 2000), we crystallized this protein complexed to the N35C mutant of gelsolin segment-1 (G1) as described by McLaughlin *et al.* (1993). The G1 system was used because the mutation sites are far away from the G1 binding sites (McLaughlin *et al.*, 1993) and also because the mutation sites are not crystal contact sites (see the section 3.3) and so it was expected that the actin-G1 crystal structure would probably reveal the mutational effects on actin structure without crystallization artifacts. The G1 system also has the advantage of not requiring a portion of actin to be chopped off by protease to obtain good crystal: in the DNase I system, it was necessary to remove the C-terminal three residues of actin by trypsin to get high-quality crystal (Kabsch *et al.*, 1990). The crystallization conditions of rabbit skeletal actin-G1 complex (Mannherz *et al.*, 1992) was helpful in finding out crystallization conditions of the *Dictyostelium* mutant actin-G1 complex. It was found that the *Dictyostelium* mutant actin crystallizes under the conditions very similar to those used in rabbit actin crystallization. The actin-G1 complex was very easy to nucleate. It was necessary to lower the protein concentration to limit the number of nucleation and produce large single crystals suitable for X-ray data collection, since the crystal nucleation is strongly dependant on protein concentration. These crystals of the full chimera diffracted past 2.4 Å resolution using synchrotron radiation. Half chimera-1, in which only residues 228-230 of *Dictyostelium* actin (QTA) were mutated to those found in *Tetrahymena* actin (KAY), crystallized under the same conditions as full chimera and gave excellent crystals that diffracted past 1.8 Å using synchrotron radiation (Figure 7). The half chimera-1 crystals had a much smaller mosaic spread (particularly along the long 180 Å *c*-axis) than full chimera crystals. Biochemical studies showed that half chimera-1 also showed higher Ca^{2+}-activation when complexed

with tropomyosin-troponin (Saeki & Wakabayashi, 2000; see Figure 6). To enable a detailed evaluation of any structural changes introduced into actin by these mutations we also obtained crystals of the wild-type actin complexed with G1 because the sequence of *Dictyostelium* actin differs from that of rabbit actin at 34 positions. The optimum pH (pH 6.6) to grow large single crystals of wild-type was slightly higher than that used in crystallization of the mutants (pH 6.0). These crystals of wild-type *Dictyostelium* actin (primarily of actin 15) diffracted past 2.4 Å resolution. Table 1 gives the lattice parameters and data collection statistics.

3.2 Structure of wild-type and mutant *Dictyostelium* actins bound to gelsolin segment-1

An atomic model of the wild-type *Dictyostelium* actin-G1 complex was obtained using molecular replacement based on the structure of the rabbit skeletal muscle actin-G1 complex (McLaughlin *et al.*, 1993). The appropriate side-chain alterations were easily fitted to the 2*Fo*–*Fc* electron density map (using omit maps where there was any ambiguity) and, after minor rebuilding, the resultant model was initially refined to an *R*-factor of 24.8 % (free-*R* 31.8 %). This model was then used to obtain a molecular replacement solution for half chimera-1, which gave a model with an *R*-factor of 18.2 % (free-*R* 22.3 %) after several cycles of rebuilding and addition of water molecules. Because the path of the main chain appeared to be slightly altered in the region mutated, residues 225-232 were built into omit maps to reduce model bias. The final 2.0 Å refined structural model for half chimera-1 was then fitted to the wild-type data using rigid body refinement and, after minor rebuilding and refinement, gave a final model for the *Dictyostelium* wild-type actin-G1 complex with an *R*-factor of 18.3 % (free-*R* 23.1 %). The 2.0 Å resolution half chimera-1 model was also used to obtain a molecular replacement solution for the full chimera. Initial rigid body refinement easily converged to an *R*-factor of 22.4 %, implying that the two mutants have similar structures. Subsequent model building and refinement cycles produced a final full mutant model with

an *R*-factor of 17.1 % (free-*R* 21.4 %). Table 2 summarizes the refinement statistics. The three models had good geometry and excellent Ramachandran plots with 93.4 – 94.5 % of residues in the most favoured regions and no residues in forbidden or generously allowed regions.

The overall molecular structure of *Dictyostelium* wild-type actin-G1 complex is shown in Figure 8. The final 2*Fo*–*Fc* electron density maps for wild-type and mutant crystals showed good density for almost all of the polypeptide chains of actin and gelsolin segment 1. However, there was no interpretable density corresponding to residues 1-2 and 43-49 of actin, indicating these regions were highly flexible and/or disordered in these crystals. Met1 of G1 was also not visible and some surface side chains of actin (Glu3, Asp4, Thr41, Lys50 and Glu270) and G1 (Arg54) were not well defined. The electron density map indicated that His73 of *Dictyostelium* actin was methylated as is the case in rabbit skeletal muscle actin. There was also a distinct positive density in the *Fo*–*Fc* difference density map indicating that His173 of *Dictyostelium* actin is probably also methylated. Methylation of His173 might play some role in actin filament formation because these histidine residues come close to each other when actin polymerizes (Holmes *et al.*, 1990; Lorenz *et al.*, 1993).

3.3 Crystal packing

We have examined crystal contact sites because the crystal structure might be affected by crystallization, although it is difficult to assess the extent of packing influence. The crystals of wild-type and mutants are isomorphous and so the mode of crystal packing is common to the three structures. Thus, the differences between wild-type and mutant structures which will be described later are not the results of different packing interactions. The actin-G1 crystal has one molecule in the asymmetric unit. Therefore, all molecules in the crystal are in identical environment regarding the crystal contacts.

The residues that interact with symmetry-related molecules are shown in black spheres in Figures 9-12. There are four molecules in the unit cell (Figure 10). Each molecule interacts not only with the neighbours in the same unit cell but also with the molecules in the next unit cells. One molecule makes contact with six neighbour molecules. The yellow molecule in Figure 11 interacts with orange, magenta, red, light green, cyan and dark green molecules in Figure 11.

The crystal contacts can be classified into five sites and we have named them sites 1, 2, 3, 4 and 5 (Table 4). In the view of Figure 11, sites 1 and 2 are clearly visible. In the site 1, Arg95 of actin subdomain 1 interacts with Ser323 of actin subdomain 3 of the molecule (related by translation) in the next unit cell. The site 2 is also an actin-actin contact site and is formed between residues Ser60, Gly63 in subdomain 2 and residues Glu195, Arg196 in subdomain 4 of a symmetry-related molecule (related by a two-fold screw axis). The sites 1 and 2 are different from the actin-actin contacts observed in filamentous actin (Figure 3) and so do not have physiological significance.

Figure 12 shows sites 3-5. The site 3 is a G1-G1 contact site and is formed between Asn69 in one molecule and Asp88, Asn91 of a symmetry-related molecule (related by a two-fold screw axis). The sites 4 and 5 are actin-G1 contact sites. In the site 4, actin residues Pro333 and Glu334 at the junction between subdomains 1 and 3 interact with G1 residues Asn56 and Gly57. The site 5 is formed between actin residues Tyr169, Arg372, Phe375 and G1 residues Tyr118, Lys120; thus, the mobility of actin C-terminus may be restricted by crystal packing.

It is important to note that the mutation sites in subdomain 4 (residues 228-230 or 228-232) do not interact with symmetry-related molecules in the crystal and are surrounded by solvent channels in the crystal. Therefore, it is reasonable to expect that the actin-G1 crystal structures reveal mutational effects on actin structure without crystal packing artifacts.

3.4 Changes introduced in chimeric actins

In the half chimera-1 mutant (Q228K/T229A/A230Y), the mutations at positions 228-230 were clear in the molecular replacement $2Fo-Fc$ electron density map (Figure 13) and were easily built into omit maps. The temperature factor of the region near the mutations was noticeably lower than in the wild-type and this greatly facilitated interpretation. Similarly, the full chimera had lower temperature factors in this region than in the wild-type and the mutations in five residues (Q228K/T229A/A230Y/A231K/S232E) were also clearly visible in the $2Fo-Fc$ map except for Lys231, for which the side chain was ill-defined and considered to be flexible. Except for the region in the vicinity of the mutations, the conformation of both chimera actins was virtually identical to that of wild-type *Dictyostelium* actin. The overall r.m.s. deviation between equivalent main chain atoms (residues 3-42 and 50-375) of any two of the three structures was less than 0.2 Å and the main chains of the three structures are almost completely superimposable (Figure 14). This similarity in overall conformation was consistent with the biochemical observation that chimeras only perturbed an "on-state" and do not affect other properties of actin: they have normal polymerizability, activate myosin ATPase normally, and do not affect an "off-state" in calcium regulation (see Figure 6). The conformation of side-chains was also strongly conserved between the three structures. Outside the region near the mutations, only the side-chains of Glu100 and Gln354 showed any significant deviation (Figure 15). These differences at Glu100 and Gln354 (which are located on the surface of subdomain 1 and so widely separated from the region mutated; see Figure 8) were not considered significant since close inspection of the $2Fo-Fc$ maps indicated that these residues probably had multiple conformations in the three structures (Figures 16 and 17). Generally, this sort of multiple conformation is often observed with surface side-chains and is characteristic of high resolution crystal structures. The two residues Glu100 and Gln354 do not directly interact with neighbouring molecules in the crystal, nor are they involved in actin-actin contacts in F-actin.

However, the conformational change of the side chain of Leu236 (Figures 15, 18 and 19) was induced by the mutations at residues 228-230 or 228-232, in addition to minor changes in the position of the main-chain atoms and a substantial decrease in temperature factor. This change was found in both chimeric actins. The movement of Leu236 appeared to be required to accommodate the side chain of Tyr230 (Figure 18) which is tucked into interior of subdomain 4, forming hydrophobic contacts with the surrounding residues (particularly Phe255). Tyr230 also forms putative hydrogen bonds with the hydroxyl group of Tyr218 and main chain carbonyl of Leu236. In the wild-type *Dictyostelium* actin structure, the side chain of Leu236 fits in a hydrophobic pocket formed by Ala230, Thr229 and Phe255 and its solvent accessibility is low (6.5 $Å^2$). The side chains of Phe255, Met227 and Phe223 closely pack against each other and form a hydrophobic core, which may stabilize the hydrophobic interaction around Phe255. The packing of Leu236 in the hydrophobic pocket is facilitated by the small size of the side chain of Ala230 of the wild-type actin. However, in both half chimera-1 and the full chimera, the bulky phenolic ring of Tyr230 fills this hydrophobic pocket, displacing the Leu236 side chain (colour coded in green in Figure 19) so that it is more exposed on the surface of subdomain 4. Figure 19 also shows that the residue 230 (colour coded in red) is more solvent accessible in the mutants than the wild-type actin. Table 5 shows that the solvent accessible surface area of Leu236 in half chimera-1 (19.6 $Å^2$) or in the full chimera (27.1 $Å^2$) is significantly larger than that in wild-type (6.5 $Å^2$) . The solvent accessibility of Leu236 in *Dictyostelium* wild-type is similar to that of rabbit skeletal muscle α-actin or cytoplasmic β-actin (5.6 - 11.2 $Å^2$) (Kabsch *et al.*, 1990; McLaughlin *et al.*, 1993; Schutt *et al.*, 1993; Chik *et al.*, 1996; Table 5). Thus, the increase in the solvent accessibility of Leu236 was shown to be induced by A230Y mutation and is not due to differences between species. This change in the environment of the Leu236 side chain appears to alter its flexibility: whereas the electron density of the Leu236 side chain was strong in wild-type *Dictyostelium* actin, it was weaker in both half chimera-1 and the full chimera. In contrast, Tyr230 has a lower temperature factor in chimeric

actins and the solvent accessible surface area of the side chain of Tyr230 is 0.3 $Å^2$ in both chimeric actins. However, the 233-236 loop (SSAL), which lies over Tyr230 and hinders access to it, has substantial flexibility (possibly because the loop is rich in serine). This flexibility could allow other proteins to access Tyr230. The side chains of Lys228 and Ala229 do not form strong interactions with other residues in half chimera-1 and project into the solvent. Therefore they do not induce any marked conformational changes in half chimera-1. In the full chimera, the same holds true for Ala229, but there was a change in the conformation of Lys228 compared with that in half chimera-1: due to an additional mutation (S232E), the side chain of Lys228 moved upward and formed a salt bridge with Glu232 in the full chimera (Figure 18c). We could identify between 394 and 469 water molecules in the different actin structures (Table 3), but there were no systematic differences in the hydration water between the three X-ray structures, indicating that the mutational effect on actin function is not associated with strongly bound water molecules.

In summary, the conformational changes in the chimeric actins (both half chimera-1 and full chimera) are restricted on the surface of the subdomain 4 in the immediate vicinity of the mutations and do not propagate along actin molecule to distal parts such as myosin binding sites or actin-actin contact sites. The two chimeric actins have a common structural feature in that A230Y mutation induces movement of Leu236.

3.5 Comparison of rabbit and *Dictyostelium* actin-G1 structures

The 2.4 Å resolution structural model of the wild-type *Dictyostelium* actin-G1 complex and the 2.0 Å or 2.4 Å resolution model obtained for the chimeric actins were remarkably similar to the 2.5 Å resolution model generated for the rabbit actin-G1 complex (McLaughlin *et al.*, 1993). The overall r.m.s. separation between equivalent main chain atoms (residues 6-39 and 50-375) in rabbit and *Dictyostelium* actin was 0.63 Å.

Therefore, although there might be some minor local conformational changes between isoforms, the overall tertiary structure of actin is strongly conserved from lower eukaryotic amoeba to higher mammals. This is consistent with the observations that *Dictyostelium* and rabbit actin show similar properties in a range of biochemical assays (Sutoh *et al.*, 1991; Saeki *et al.*, 1996). Moreover, this observation is consistent with difference between actins in complex with different actin-binding proteins (Kabsch *et al.*, 1990; Schutt *et al.*, 1993; McLaughlin *et al.*, 1993) being due primary to differences introduced by the different binding proteins or by crystal packing.

The level of similarity between the rabbit and *Dictyostelium* actin structures was remarkable considering that they differ at 34 positions (Sheterline *et al.*, 1996). Although many of the mutated residues were located on the surface of actin and so were partially or fully solvent accessible, others were buried in hydrophobic core of subdomains. Residues 1-4 are completely exposed to solvent and have high temperature factors (above 70 $Å^2$) and are probably very flexible. In rabbit actin, Thr5 and Thr6 do not form any specific contact with the rest of actin molecule and seem to be flexible. By contrast, in *Dictyostelium* actin, the side chain of Val5 makes hydrophobic interaction with the aliphatic ring of Pro102 and the side chain of Gln6 forms hydrogen bonds with the main chain carbonyls of Ala7 and Ala22. Therefore, the mobility of N-terminal residues of *Dictyostelium* actin may be more restricted than that in rabbit actin. Among the other exterior mutations, five residues are potentially involved in actin-actin contact in F-actin. They are residues 41, 201, 260, 267 and 287 (Holmes *et al.*, 1990; Lorenz *et al.*, 1993). These mutations could modulate interaction between actin protomers in actin filaments. Several internal substitutions occur in close vicinity each other: they are in subdomain 1 (residues 10, 17 and 76), subdomain 3 (residues 153, 160, 162, 297, 299 and 317) and subdomain 4 (residues 189 and 217) and tend to compensate each other's effect on structure. For example, the volume change in the side chain of the residue 153 (L153M) is compensated by a mutation in a neighbouring residue (T160S). Thus, rabbit/*Dictyostelium* actin sequence differences in interior core are such that they hardly

alter the three-dimensional actin fold. These changes are consistent with recent studies that indicated that the structure of each actin subdomain is strongly conserved, even when the overall structure changes between "open" and "tight" forms (Page *et al.*, 1998).

3.6 ATP Interactions

The higher resolution data obtained in this study enabled the identification of between 394 and 469 bound waters in the different actin structures (Table 3) and also enabled the interactions between actin and ATP to be defined more precisely. The structural description below is based on the 2.0 Å resolution structure of ATP binding site in half chimera-1 actin, but the structure of this region was almost the same in wild-type or the full chimera, and so the structure here is not influenced by mutations in subdomain 4. The nucleotide binding cleft of actin is filled with water molecules. Figure 20 shows that actin recognizes hydrated forms of both the Ca^{2+} ion and the adenine base in the nucleotide binding site. Ca^{2+}ATP interacts with actin through an extensive hydrogen bond network, in which several water molecules are involved. The four nitrogen atoms of the adenine base (N1, N3, N6 and N7) in a hydrophobic pocket (which is formed mainly by Met305, Phe306 and the aliphatic part of the side-chain of Glu214) are hydrogen-bonded to polar groups on actin through intervening water molecules. These hydrogen bond networks mediated by water molecules appear to stabilize binding of the adenine base and make the interaction more stereospecific: thus actin recognizes the hydrated form of the adenine base. The interaction of ribose ring and phosphate groups with actin is broadly similar to that described by Kabsch *et al.* (1990). However, the water molecules that bridge the Ca^{2+} ion and actin residues are notable. The Ca^{2+} ion has typical pentagonal bipyramidal coordination pattern, which is by far the most prevalent coordination geometry observed in the calcium binding sites of proteins (McPhalen *et al.*, 1991) and is liganded by seven oxygen atoms. Two of the seven ligands are oxygen atoms of β- and γ-phosphate. The other five ligands are all water molecules. The hydrophilic residues Asp11, Gln137 and Asp154, which were noted by Kabsch *et al.*

(1990) to form a hydrophilic pocket around the Ca^{2+} but which are too far away to form direct contact with the Ca^{2+} are now found to coordinate with the Ca^{2+} through intervening water molecules. Thus actin recognizes a hydrated Ca^{2+} ion in the nucleotide binding site.

ATP hydrolysis by actin is intimately associated with its polymerization and is important for the dynamics of actin filaments (Korn *et al.*, 1987). It is most likely that the ATP hydrolysis occurs by nucleophilic attack of a water molecule on the γ-phosphorus from the opposite side of the β–γ bond. The water molecule which lies approximately in-line to the β–γ bond and is in the closest position to the γ-phosphorus is Wat203, which forms hydrogen bonds with side-chain carbamoyl group of Gln137 and two nearby water molecules (Figure 21). However, the distance between Wat203 and the γ-phosphorus is 4.74 Å, which is probably too large to perform an in-line nucleophilic attack effectively. Thus, there is no clear candidate for a nucleophile in ATP hydrolysis in the Ca^{2+}ATP-form crystal structure and it seems that the hydrolysis of ATP by Ca^{2+}-actin requires substantial conformational changes and rearrangement of water molecules around the γ-phosphate. This is consistent with the extremely low intrinsic ATPase activity of Ca^{2+}-G-actin (Estes *et al.*, 1992).

4. Discussion

We have established the crystal structures of wild-type *Dictyostelium* actin, half chimera-1 and the full chimera in complex with gelsolin segment 1 to resolutions of 2.4 Å, 2.0 Å and 2.4 Å, respectively. The structural models obtained have excellent geometry and establish the local structural changes present in the mutants in atomic detail. It was also shown that actin recognizes the hydrated form of the adenine base and the Ca^{2+} ion in the nucleotide binding pocket.

4.1 Roles of Leu236 and Tyr230 in the interaction between actin and tropomyosin-troponin

In half chimera-1, residues 228-230 (QTA) of wild-type *Dictyostelium* actin are mutated to the sequence KAY found in *Tetrahymena* actin. These changes result in half chimera-1 showing almost the same higher Ca^{2+}-activation (4-fold greater than wild-type) of the regulated acto-myosin S1 ATPase (Saeki & Wakabayashi, 2000; see Figure 6) as observed previously for the full chimera (Saeki *et al.*, 1996). Moreover, it has recently been demonstrated, using a range of point mutants in this region of *Dictyostelium* actin (Saeki & Wakabayashi, 2000), that the mutation A230Y is sufficient to produce the higher Ca^{2+}-activation (Figure 6). These biochemical results are consistent with the observation that, in the crystal structures of both half chimera-1 and the full chimera, the A230Y mutation causes a similar local conformational change in subdomain 4 (Figures 18 and 19). Thus, both the structural and biochemical results suggest that the movement of the side chain of Leu236 induced by the A230Y mutation and/or the introduction of the aromatic tyrosine side chain at residue 230 must be primarily responsible for the higher Ca^{2+}-activation of the myosin S1 ATPase by these mutant actins in the presence of tropomyosin and troponin.

As shown in Figure 19, the side chains of both Leu236 and the Tyr230 in the

mutants show increased solvent accessibility compared with wild-type actin. To examine which residue was more important in producing the increased Ca^{2+}-activation, we used protein engineering to introduce an additional mutation (L236A) into half chimera-1 (Saeki *et al.*, unpublished data). If Leu236 was more important, truncation of its side chain should reduce the Ca^{2+}-activation, whereas if Tyr230 was more important, this truncation would increase the accessibility to Tyr230 and so result in either the same or higher Ca^{2+}-activation. It was found that the latter is the case: the additional L236A mutation produced a substantially higher Ca^{2+}-activation than the other mutants and showed a 14-fold increase over that observed with wild-type actin, whereas both half chimera-1 and the full chimera showed only a 4-fold increase. These data indicate strongly that Tyr230 interacts directly with the regulatory proteins to facilitate Ca^{2+}-activation. Significantly, the additional L236A mutation did not affect the unregulated acto-S1 ATPase activity (i.e., that with only actin) or the regulated acto-S1 ATPase activity in the absence of Ca^{2+} (data not shown) indicating that this mutation had altered only the Ca^{2+}-activation. In summary, the data obtained with the L236A mutant of half chimera-1 indicates that the presence of Tyr230 is probably more important than the movement of the side chain of Leu236 in generating the higher Ca^{2+}-activation observed with the chimeric actins.

4.2 Relation between higher Ca^{2+}-activation and the binding of tropomyosin-troponin to actin

Unlike the full chimera, both half chimera-1 and the A230Y mutant show a similar affinity for both tropomyosin alone or for the tropomyosin-troponin complex (with or without Ca^{2+}) as observed with wild-type actin. Recently the affinity of mutant actins for tropomyosin was measured quantitatively (Saeki & Wakabayashi, 2000; see Table 6) and it was found that the wild-type and all mutants bind tropomyosin in the same stoichiometry (saturable at an actin:Tm molar ratio of 7:1) and that the apparent dissociation constant (K_{app}) of the half chimera (1.03 ± 0.17 μM) was almost the same as

that for wild-type actin (0.95 ± 0.09 μM), whereas the full chimera showed a slightly lower affinity (1.65 ± 0.17 μM), consistent with that reported previously (Saeki *et al.*, 1996). Thus there was no correlation between the strength of tropomyosin binding and the Ca^{2+}-activation observed. It may be that the equilibrium binding assay between actin and tropomyosin is not measuring the interaction important for the Ca^{2+}-activation. The binding of tropomyosin-troponin complex to actin is three orders of magnitude stronger than binding of tropomyosin alone to actin (Dahiya *et al.*, 1994) and co-sedimentation experiments did not show any marked differences among the three actins in binding of tropomyosin-troponin complex to actin both in the presence and absence of Ca^{2+} (Saeki *et al.*, 1996; Saeki & Wakabayashi, 2000). Similarly, the additional mutation L236A into half chimera-1 did not substantially affect the affinity of actin to tropomyosin or tropomyosin-troponin complex: K_{app} of the actin-tropomyosin binding of this mutant actin was 0.87 ± 0.04 μM (Saeki *et al.*, unpublished data). Therefore, if the higher Ca^{2+}-activation of regulated acto-S1 ATPase activity observed in the mutants containing Tyr230 is due to the stabilization of interaction between actin and regulatory proteins, it does not seem to be related to altering the strength of actin-regulatory protein binding in these functional states of thin filaments, because half chimera-1 shows essentially the same tropomyosin affinity as the wild type. It appears more plausible that the A230Y mutation facilitates *transition* of tropomyosin to the site where, together with troponin, it induces higher Ca^{2+}-activation. In this case, the overall affinity of tropomyosin for actin would not be correlated necessarily with Ca^{2+}-activation.

4.3 The role of Tyr230 in the higher Ca^{2+}-activation

The results we have obtained with the actin chimeras can be accounted for in the context of the three-state model for the activation of muscle thin filaments (see Figure 4 and Table 1; McKillop & Geeves, 1993; Lehrer, 1994; Geeves & Conibear, 1995; for a review, see Holmes, 1995). Although the biochemical data based on which the three-state model was deduced were taken with rabbit skeletal actin and not with

Dictyostelium actin, the three-state model probably also applies to thin filaments reconstructed using *Dictyostelium* actin because rabbit and *Dictyostelium* actins show essentially the same properties in any of the functional assay (Saeki *et al.*, 1996). In the three-state model, tropomyosin is proposed to occupy three different states: a "blocked" state, in which it is located at a high radius in the F-actin groove and completely inhibits the binding of myosin S1 heads to actin; a "closed" state in which it is located at lower radius and which allows the weak S1-actin interaction but not the strong S1-actin interaction required to generate tension; and an "open" state where both weak and strong S1-actin interactions can occur. The "blocked" state would correspond to the absence of Ca^{2+} when the myosin S1 ATPase is not activated, whereas the "open" and "closed" states are observed in the presence of Ca^{2+}. However, the transition from "closed" to "open" state requires binding of S1 and probably is associated with tropomyosin changing its position slightly in the actin groove (McKillop & Geeves, 1993; Lehrer, 1994; Geeves & Conibear, 1995; for a review, see Holmes, 1995). The transition from a "closed state" to an "open state" does not appear to occur easily in wild-type actin and so regulated acto-S1 ATPase is not maximally activated in the presence of Ca^{2+} in wild-type actin (Figure 6). A large body of evidence indicates that the region in subdomain 4 around residue 230 is located at or near one of the sites on the surface of actin filaments where tropomyosin binds in the "open" (or "on") state when both Ca^{2+} ions and myosin S1 heads are present (Toyoshima & Wakabayashi, 1985; Milligan *et al.*, 1990; Vibert *et al.*, 1997; see Figure 22). The region is also close to the site of binding of tropomyosin to actin in the absence of troponin which appears to correspond to the "closed state" (Wakabayashi *et al.*, 1975; Lorenz *et al.*, 1995; Ishikawa & Wakabayashi, 1999). Tropomyosin is probably also located in this position in the presence of troponin and Ca^{2+} but without myosin heads (Lehman *et al.*, 1994; Ishikawa & Wakabayashi, 1994; Al-Khayat *et al.*, 1995; Lehman *et al.*, 1995; Vibert *et al.*, 1997; Xu *et al.*, 1999).

The higher Ca^{2+} activation observed with constructs containing the A230Y mutation can be most easily interpreted as increasing the frequency with which

tropomyosin occupies the "open" state essential for activation of the myosin S1 ATPase. Such an increased occupancy of the "open" state could result from either Tyr230 stabilizing the "open" state or destabilizing one or both of the other states. Although in principle Tyr230 could decrease the stability of the "blocked" state (and so increase the total "closed" and "open" population in the presence of Ca^{2+}), this would seem unlikely because electron microscopy has indicated that, in the absence of Ca^{2+}, tropomyosin is located at high radius in thin filaments and probably does not bind to subdomain 4, in which residue 230 is located (Toyoshima & Wakabayashi, 1985; Milligan *et al.*, 1990; Vibert *et al.*, 1997). Instead it would appear more likely that Tyr230 mutants would either decrease the stability of the "closed" state or increase the stability of the "open" state. For example, the "closed" state would be destabilized if the A230Y mutation interfered with the tropomyosin-actin interaction for this state (thus, enabling myosin S1 to more easily "push" the tropomyosin into the "open" state), whereas the "open" state would be stabilized if the A230Y mutation increased the strength of the actin-tropomyosin interaction for this state.

Because the A230Y mutants do not show the consistent pattern of weaker binding to tropomyosin which would be expected if the mutation were to destabilize the "closed" state (which is thought to correspond to the position occupied by tropomyosin in the absence of troponin, see Wakabayashi et al., 1975; Lorenz et al., 1995; Ishikawa & Wakabayashi, 1999), it appears more likely that Tyr230 is instead stabilizing the "open" state. One way in which this could be achieved would be for the aromatic ring of Tyr230 to form hydrophobic contacts with hydrophobic zones on tropomyosin. Hydrophobic residues often play key roles in interaction interfaces between proteins (Jones & Thornton, 1997; Larsen, *et al.*, 1998; Tsai *et al.*, 1997) and tyrosine residues are frequently present in hydrophobic hot spots that are important for many protein-protein interactions (Bogan & Thorn, 1998). Moreover tropomyosin has a repeating pattern of hydrophobic residues on its outer surface that has the same spacing as the zones of negative charge associated with actin binding (Stewart & McLachlan, 1975; McLachlan & Stewart, 1976; see Figure 23).

An interaction between these outer hydrophobic zones on tropomyosin and Tyr230 on actin would certainly account for the increased Ca^{2+}-activation observed in the chimeric actins. Therefore, it is certainly plausible that position 230 on actin forms part of the tropomyosin binding site in the "open" state and so the A230Y could facilitates the azimuthal movement of tropomyosin from the "closed" to the "open" state and so increase the level of Ca^{2+}-activation. Although in principle Tyr230 might instead contact directly with troponin-T (because troponin-T probably lies near tropomyosin and it has been suggested that troponin-T directly binds to actin and plays an important role to confer calcium sensitivity to the regulatory system (Dahiya *et al.*, 1994; Perry, 1998)), it is less easy to account for the increased Ca^{2+}-activation if this were the case, since troponin is probably primarily responsible for the Ca^{2+}-induced transition from "blocked" to "closed" states whereas the transition from "closed" to "open" states appears to involve tropomyosin being pushed by S1 heads (reviewed by Holmes, 1995). The nature of the putative interaction between Tyr230 and tropomyosin or troponin may not be merely hydrophobic but may have a tyrosine-specific feature, because the higher Ca^{2+}-activation was not observed in wild-type actin, in which hydrophobic side chain of Leu236 occupies almost the same position as Tyr230 in the mutants and is partially exposed on the surface.

The higher Ca^{2+}-activation seen with the Tyr230-containing mutant actins (i.e., half chimera-1, the full chimera and the A230Y mutant) requires both tropomyosin and troponin. In the absence of troponin, the acto-S1 ATPase is partially inhibited by tropomyosin in wild-type actin and the extent of this partial inhibition is almost the same as in wild-type for Tyr230-containing mutants (half chimera-1, the full chimera and the A230Y mutant (Saeki & Wakabayashi, 2000)). It is only when both of tropomyosin and troponin (+ Ca^{2+}) are present that the acto-S1 ATPase activity is enhanced by Tyr230-containing mutant actins. This indicates that the critical trigger for the higher Ca^{2+}-activation observed in these mutants is the increased population of tropomyosin interacting with actin around the actin residue 230 and that this also requires the presence of troponin. In the mutants which have tyrosine at residue 230 but have leucine at

residue 236, Leu236 may partially inhibit the putative Tyr230-tropomyosin interaction. In such mutants, troponin might help to displace S233-L236 loop so that tropomyosin can access Tyr230 more easily. In the wild-type structure, the S233-L236 loop can be thought of as being "anchored" by L236 fitting in the nonpolar pocket, but L236 is displaced from the nonpolar pocket by A230Y mutation in the mutants so that the anchoring of S233-L236 loop is weaker in the mutant structures. Therefore it is conceivable that the S233-L236 loop can be displaced by regulatory proteins without great difficulty in the thin filaments consisting of the Tyr230-containing mutant actins and tropomyosin-troponin.

4.4 Why *Tetrahymena* actin does not bind tropomyosin?

Tetrahymena actin is one of the most unique actins among the actins known at present. *Tetrahymena* actin shares about 75 % amino acid sequence homology with rabbit or *Dictyostelium* actins (Table 7). This value is extremely low as a homology rate between known actins. Although rabbit and *Dictyostelium* actins bind tropomyosin normally, *Tetrahymena* actin does not bind tropomyosin (Hirono *et al.*, 1990). The region around residue 230 is the most divergent region when *Tetrahymena* actin is compared with other actins which bind tropomyosin normally except for the N-terminus where identity is generally low among species (Figure 24). This was one of the original motivations to construct the *Dictyostelium* mutant actins in which only the residues around 230 are replaced with *Tetrahymena* sequence and to see what happens regarding tropomyosin binding and Ca^{2+}-regulation (Saeki *et al.*, 1996; Saeki & Wakabayashi, 2000). Rather unexpectedly, the replacement of residues 228-232 (i. e., the full chimera) did not show substantially lower affinity for tropomyosin compared with wild-type actin (Saeki & Wakabayashi, 2000). Thus, the residues 228-232 may not be the major determinant of the overall affinity of actin for tropomyosin alone and so the other mutations in *Tetrahymena* actin may be responsible for the inability of *Tetrahymena* actin to bind tropomyosin (Figures 24 and 25). Many residues are simultaneously mutated in

Tetrahymena actin but there are few changes in surface charges in the regions that are proposed to be the tropomyosin binding sites (Wakabayashi *et al.*, 1975; Lorenz *et al.*, 1995; Ishikawa & Wakabayashi, 1999) except for the region around residue 230. Therefore, non-electrostatic interactions may also be important for the actin's overall affinity for tropomyosin in addition to the charge-charge interactions that are proposed to be critical in actin-tropomyosin binding (McLachlan & Stewart, 1976; Lorenz *et al.*, 1995).

Tetrahymena actin has the ability to copolymerize with skeletal actin and to bind myosin S1 in the same ATP-dependant manner as skeletal actin (Hirono *et al.*, 1990). Thus, the overall structure of *Tetrahymena* actin does not seem to be dramatically different from that of skeletal muscle actin. This can also be inferred from the fact that the amino acid substitutions found in the hydrophobic cores of *Tetrahymena* actin are mostly conservative as noted by Hirono *et al.* (1987).

If our proposal that the side-chain of Tyr230 directly interacts with tropomyosin and strengthens the interaction with tropomyosin is true, there must be some factors which prevent this to occur in *Tetrahymena* actin. There are mutations at residues 235 and 236 in *Tetrahymena* actin and these side-chains may hinder access to Tyr230. It is also notable that some residues around residue 250 which lie behind Tyr230 are mutated in *Tetrahymena* actin; this may induce local conformational changes in subdomain 4. Anyway, the understanding of structure-function relationship in *Tetrahymena* actin requires atomic structure of *Tetrahymena* actin. However, it may be difficult to crystallize *Tetrahymena* actin in the G1 system because there are some mutations in amino acid residues involved in crystal packing in the G1 system.

4.5 Suggestions for future experiments

One of the key suggestions raised by this work is that the A230Y mutation may

stabilize the actin-tropomyosin interaction in the "open-state." This could be tested by binding assay of tropomyosin to actin filaments fully decorated with rigor-type myosin heads.

Although the effects of mutations on Ca^{2+}-regulation were assessed so far by steady-state ATPase activities of regulated acto-S1 or nonregulated acto-S1, it is important to further characterize the mutational effects by *in vitro* motility assay because the coupling between ATPase and sliding movement is important. The ATPase activity is just an indirect indicator of contractile events.

As discussed extensively in this thesis, the region around residue 230 is probably important in actin-tropomyosin interaction in the fully activated thin filaments. It would be interesting to monitor this interaction by fluorescent probe attached to a site near residue 230. One method to introduce fluorescent probe is to introduce a cystein residue on the actin surface and attach a cystein-specific fluorescent dye. The position to introduce the probe will be critical: the probe must be close enough to the binding site to sense the presence of tropomyosin but not so close to the binding site that it interferes with actin-tropomyosin binding. The crystal structures of the mutant actins described in this thesis would certainly help to design such a new mutant actin.

Finally, one of the great future challenges is to solve the structure of actin-tropomyosin-troponin complex at atomic resolution. Lower resolution images are already available but the understanding of the detailed molecular mechanism requires the atomic structure of the complex. To crystallize actin-tropomyosin-troponin complex, it is necessary to develop a method to prepare short segments of the thin filament of a homogeneous length distribution.

5. Conclusions

In summary, the structure of the *Dictyostelium* half chimera-1 and full chimera suggest that the higher Ca^{2+}-activation of myosin S1 ATPase observed in these mutant actins in the presence of tropomyosin-troponin and Ca^{2+} is a consequence of local changes on the surface of subdomain 4 which probably lead to modulation of hydrophobic interactions between actin and tropomyosin-troponin in the presence of Ca^{2+}. Position 230 on actin clearly has a key role in this higher Ca^{2+}-activation and appears to form part of the interface on actin that binds directly to tropomyosin in thin filaments in actively contracting muscle.

Acknowledgements

I am grateful to Professor Takeyuki Wakabayashi for helpful and informative guidance throughout this study. I thank Dr. Murray Stewart for his excellent guidance in X-ray crystallography. I thank Mr. Takuo Yasunaga for his help in data analysis. I am indebted to Ms. Kimiko Saeki for her technical assistance in biochemistry. I am grateful to Dr. Alan Weeds for the generous gift of expression vector for G1. I thank Dr. Andrew Leslie for assistance in data processing. The data collection for the half chimera-1 crystal was performed at the SPring-8 with the approval of the Japan Synchrotron Radiation Research Institute (JASRI) (Proposal No. 1998A0222-NL -np); I thank Dr. Masahide Kawamoto and Dr. Nobuo Kamiya for their help in data collection at SPring-8. I am indebted to the staff at the Photon Factory for help in data collection of the full chimera crystal. Finally, I thank all my colleagues for many helpful comments, valuable advice and stimulating discussions.

References

AL-Khayat, H. A., Yagi, N. & Squire, J. M. (1995). Structural changes in actin-tropomyosin during muscle regulation: computer modeling of low-angle X-ray diffraction data. *J. Mol. Biol.* **252**, 611-632.

Bogan, A. A. & Thorn, K. S. (1998). Anatomy of hot spots in protein interfaces. *J. Mol. Biol.* **280**, 1-9.

Brünger, A. T. (1992). Free *R* value: a novel statistical quantity for assessing the accuracy of crystal structures. *Nature* **355**, 472-475.

CCP4 (1994). The CCP4 suite: programs for protein crystallography. *Acta Crystallog. sect. D* **50**, 760-763.

Chik, J. K., Lindberg, U. & Schutt, C. E. (1996). The structure of an open state of β-actin at 2.65Å resolution. *J. Mol. Biol.* **263**, 607-623.

Collins, J. H. & Elzinga, M. (1975). The primary structure of actin from rabbit skeletal muscle. Completion and analysis of the amino acid sequence. *J. Biol. Chem.* **250**, 5915-5920.

Dahiya, R., Butters, C. A. & Tobacman, L. S. (1994). Equilibrium linkage analysis of cardiac thin filament assembly. Implications for the regulation of muscle contraction. *J. Biol. Chem.* **269**, 29457-29461.

Ebashi, S., Endo, M. & Ohtsuki, I. (1969). Control of muscle contraction. *Q. Rev. Biophys.* **2**, 351-384.

Ebashi, S. & Endo, M. (1968). Calcium ions and muscle contraction. *Prog. Biophys. Mol. Biol.* **18**, 123-183.

Estes, J. E., Selden, L. A., Kinosian, H. J. & Gershman, L. C. (1992). Tightly-bound divalent cation of actin. *J. Muscle Res. Cell Motil.* **13**, 272-284.

Geeves, M. A. & Conibear, P. B. (1995). The role of three-state docking of myosin S1 with actin in force generation. *Biophys. J.* **68**, 194s-201s.

Geeves, M. A. (1991). The dynamics of actin and myosin association and the crossbridge model of muscle contraction. *Biochem. J.* **274**, 1-14.

Haselgrove, J. C. (1972). X-ray evidence for a conformational change in the actin-containing filaments of vertebrate striated muscle. *Cold Spring Harbor Symp. Quant. Biol.* **37**, 341-352.

Hirono, M., Tanaka, R. & Watanabe, Y. (1990). *Tetrahymena* actin: copolymerization with skeletal muscle actin and interactions with muscle actin-binding proteins. *J. Biochem.* **107**, 32-36.

Hirono, M., Endoh, H., Okada, N., Numata, O. & Watanabe, Y. (1987). *Tetrahymena* actin. Cloning and sequencing of the *Tetrahymena* actin gene and identification of its gene product. *J. Mol. Biol.* **194**, 181-192.

Holmes, K. C., Popp, D., Gebhard, W. & Kabsch, W. (1990). Atomic model of the actin filament. *Nature* **347**, 44-49.

Holmes, K. C. (1995). The actomyosin interaction and its control by tropomyosin. *Biophys. J.* **68**, 2s-7s.

Huxley, H. E. (1972). Structural changes in the actin- and myosin-containing filaments during contraction. *Cold Spring Harbor Symp. Quant. Biol.* **37**, 361-376.

Huxley, A. F. & Neidergerke, R. (1954). Structural changes during muscle contraction. Interference microscopy of living muscle fibres. *Nature* **173**, 971-972.

Huxley, H. E. & Hanson, J. (1954). Changes in the cross-striations of muscle during contraction and stretch and their interpretation. *Nature* **173**, 973-976.

Ishikawa, T. & Wakabayashi, T. (1994). Calcium induced change in three-dimensional structure of thin filaments of rabbit skeletal muscle as revealed by cryo-electron microscopy. *Biochem. Biophys. Res. Commun.* **203**, 951-958.

Ishikawa, T. & Wakabayashi, T. (1999). Calcium-induced changes in the location and conformation of troponin in skeletal muscle thin filaments. *J. Biochem.* **126**, 200-211.

Johara, M., Toyoshima, Y. Y., Ishijima, A., Kojima, H., Yanagida, T. & Sutoh, K. (1993). Charge-reversion mutagenesis of *Dictyostelium* actin to map the surface recognized by myosin during ATP-driven sliding motion. *Proc. Natl. Acad. Sci. USA* **90**, 2127-2131.

Jones, S. & Thornton, J. M. (1997). Prediction of protein-protein interaction sites using patch analysis. *J. Mol. Biol.* **272**, 133-143.

Jones, T. A., Zou, J. -Y., Cowan, S. W. & Kjeldgaard, M. (1991). Improved methods for building protein models in electron density maps and for locating errors in these models. *Acta Crystallog. sect. A* **47**, 110-119.

Kabsch, W. & Holmes, K. C. (1995). The actin fold. *FASEB J.* **9**, 167-174.

Kabsch, W., Mannherz, H. G., Suck, D., Pai, E. F. & Holmes, K. C. (1990). Atomic structure of the actin:DNase I complex. *Nature* **347**, 37-44.

Kabsch, W. (1976). A solution for the best rotation to relate two sets of vectors. *Acta Crystallog. sect. A* **32**, 922-923.

Kamiya, N., Uruga, T., Kimura, H., Yamaoka, H., Yamamoto, M., Kawano, Y., Ishikawa, T., Kitamura, H., Ueki, T., Iwasaki, H., Kashihara, Y., Tanaka, N., Moriyama, H., Hamada, K., Miki, K., & Tanaka, I. (1995). Fundamental design of the high energy undulator pilot beamline for macromolecular crystallography at the SPring-8. *Rev. Sci. Inst.* **66**, 1703-1705.

Korn, E. D., Carlier, M. -F. & Pantaloni, D. (1987). Actin polymerization and ATP hydrolysis. *Science* **238**, 638-644.

Kraulis, P. J. (1991). MOLSCRIPT: a program to produce both detailed and schematic plots of protein structures. *J. Appl. Cryst.* **24**, 946-950.

Larsen, T. A., Olson, A. J. & Goodsell, D. S. (1998). Morphology of protein-protein interfaces. *Structure* **6**, 421-427.

Lehman, W., Craig, R. & Vibert, P. (1994). Ca^{2+}-induced tropomyosin movement in *Limulus* thin filaments revealed by three-dimensional reconstruction. *Nature* **368**, 65-67.

Lehman, W., Vibert, P., Uman, P. & Craig, R. (1995). Steric-blocking by tropomyosin visualized in relaxed vertebrate muscle thin filaments. *J. Mol. Biol.* **251**, 191-196.

Lehrer, S. S. (1994). The regulatory switch of the muscle thin filament: Ca^{2+} or myosin heads? *J. Muscle Res. Cell Motil.* **15**, 232-236.

Lorenz, M., Popp, D. & Holmes, K. C. (1993). Refinement of the F-actin model against X-ray fiber diffraction data by the use of a directed mutation algorithm. *J. Mol. Biol.* **234**, 826-836.

Lorenz, M., Poole, K. J. V., Popp, D., Rosenbaum, G. & Holmes, K. C. (1995). An atomic model of the unregulated thin filament obtained by X-ray fiber diffraction on oriented actin-tropomyosin gels. *J. Mol. Biol.* **246**, 108-119.

Mannherz, H. G., Gooch, J., Way, M., Weeds, A. G. & McLaughlin, P. J. (1992). Crystallization of the complex of actin with gelsolin segment 1. *J. Mol. Biol.* **226**, 899-901.

Matsuura, Y., Stewart, M., Kawamoto, M., Kamiya, N., Saeki, K., Yasunaga, T. & Wakabayashi, T. (2000). Structural basis for the higher Ca^{2+}-activation of the regulated actin-activated myosin ATPase observed with *Dictyostelium/Tetrahymena* actin chimeras. *J. Mol. Biol.* **296**, 579-595.

McKillop, D. F. A. & Geeves, M. A. (1993). Regulation of the interaction between actin and myosin subfragment-1: evidence for three states of the thin filament. *Biophys. J.* **65**, 693-701.

McLachlan, A. D. & Stewart, M. (1976). The 14-fold periodicity in α-tropomyosin and the interaction with actin. *J. Mol. Biol.* **103**, 271-298.

McLaughlin, P. J., Gooch, J. T., Mannherz, H. G. & Weeds, A. G. (1993). Structure of gelsolin segment 1-actin complex and the mechanism of filament severing. *Nature* **364**, 685-692.

McPhalen, C. A., Strynadka, N. C. J. & James, M. N. G. (1991). Calcium-binding sites in proteins: a structural perspective. *Adv. Protein Chem.* **42**, 77-144.

Merritt, E. A. and Bacon, D. J. (1997). Raster3D: photorealistic molecular graphics. *Methods Enzymol.*, **277**, 505-524

Milligan, R. A., Whittaker, M. & Safer, D. (1990). Molecular structure of F-actin and location of surface binding sites. *Nature* **348**, 217-221.

Otwinowski, Z. & Minor, W. (1997). Processing of X-ray diffraction data collected in oscillation mode. *Methods Enzymol.* **276**, 307-326.

Page, R., Lindberg, U. & Schutt, C. E. (1998). Domain Motions in Actin. *J. Mol. Biol.* **280**, 463-474.

Parry, D. A. D. & Squire, J. M. (1973). Structural role of tropomyosin in muscle regulation: analysis of the X-ray diffraction patterns from relaxed and contracting muscles. *J. Mol. Biol.* **75**, 33-55.

Perry, V. (1998). Troponin T: genetics, properties and function. *J. Muscle Res. Cell Motil.* **19**, 575-602.

Rayment, I., Holden, H. M., Whittaker, M., Yohn, C. B., Lorenz, M., Holmes, K. C. & Milligan, R. A. (1993). Structure of the actin-myosin complex and its implications for muscle contraction. *Science* **261**, 58-65.

Romans, P. & Firtel, R. A. (1985). Organization of the actin multigene family of *Dictyostelium discoideum* and analysis of variability in the protein coding regions. *J. Mol. Biol.* **186**, 321-335.

Saeki, K., Sutoh, K. & Wakabayashi, T. (1996). Tropomyosin-binding site(s) on the *Dictyostelium* actin surface as identified by site-directed mutagenesis. *Biochemistry* **35**, 14465-14472.

Saeki, K. & Wakabayashi, T. (2000). A230Y mutation of actin on subdomain 4 is sufficient for higher calcium activation of actin-activated myosin ATPase in the presence of Tropomyosin-Troponin. *Biochemistry* **39**, 1324-1329.

Schaertl, S., Lehrer, S. S. & Geeves, M. A. (1995). Separation and characterization of the two functional regions of troponin involved in muscle thin filament regulation. *Biochemistry* **34**, 15890-15894.

Schutt, C. E., Myslik, J. C., Rozycki, M. D., Goonesekere, N. C. W. & Lindberg, U. (1993). The structure of crystalline profilin-β-actin. *Nature* **365**, 810-816.

Sheterline, P., Clayton, J. & Sparrow, J. C. (1996). *Protein Profile*: Actin (3rd Ed.) Academic press Inc., San Diego.

Squire, J. M. & Morris, E. P. (1998). A new look at thin filament regulation in vertebrate skeletal muscle. *FASEB. J.* **12**, 761-771.

Squire, J. (1981). The structural basis of muscular contraction. Plenum Press, New York.

Stewart, M. & McLachlan, A. D. (1975). Fourteen actin-binding sites on tropomyosin? *Nature* **257**, 331-333.

Sutoh, K., Ando, M. & Toyoshima, Y. Y. (1991). Site-directed mutations of *Dictyostelium* actin: disruption of a negative charge cluster at the N terminus. *Proc. Natl. Acad. Sci. USA* **88**, 7711-7714.

Toyoshima, C. & Wakabayashi, T. (1985). Three-dimensional image analysis of the complex of thin filaments and myosin molecules from skeletal muscle. V Assignment of actin in the actin-tropomyosin-myosin subfragment-1 complex. *J. Biochem.* **97**, 245-263.

Tsai, C. -J., Lin, S. L., Wolfson, H. J. & Nussinov, R. (1997). Studies of protein-protein interfaces: a statistical analysis of the hydrophobic effect. *Protein Sci.* **6**, 53-64.

Vandekerckhove, J. & Weber, K. (1980). Vegetative *Dictyostelium* cells containing 17 actin genes express a single major actin. *Nature* **276**, 720-721.

Vibert, P., Craig, R. & Lehman, W. (1997). Steric-model for activation of muscle thin filaments. *J. Mol. Biol.* **266**, 8-14.

Wakabayashi, T., Huxley, H. E., Amos, L. A. & Klug, A. (1975). Three-dimensional image reconstruction of actin-tropomyosin complex and actin-tropomyosin-troponin T-troponin I complex. *J. Mol. Biol.* **93**, 477-497.

Whitby, F. Kent, H., Stewart, F., Stewart, M., Xie, X., Hatch, V., Cohen, C. & Phillips, G. N. (1992). Structure of tropomyosin at 9 Å resolution. *J. Mol. Biol.* **227**, 441-452.

Xu, C., Craig, R., Tobacman, L., Horowitz, R. & Lehman, W. (1999). Tropomyosin positions in regulated thin filaments revealed by cryoelectron microscopy. *Biophys. J.* **77**, 985-992.

Figure legends

Figure 1. Skeletal muscle contraction and its regulation by Ca^{2+} ions. The skeletal muscle comprises long, cylindrical muscle fibres (about 100 μm across), each of which is a single multinuclear muscle cell. Each fibre contains a bundle of parallel cylindrical myofibrils (about 2 to 3 μm across) mainly composed of the contractile material. This material is organized into repeating units, the sarcomeres, which are commonly about 2 to 3 μm long. This gives the myofibrils, the fibres, and the whole muscle their characteristic cross-striated appearance. Muscle contraction occurs when thick and thin filaments slide past each other. Thick filaments are mainly composed of myosin molecules. The long tail of myosin molecule is responsible for the assembly of myosin molecules into filaments. The globular heads of myosin project outwards from the thick filaments and contain the ATPase site and actin-binding sites. Thin filaments are composed of actin, tropomyosin and troponin. This figure was adapted from Squire (1981) and Ebashi *et al.* (1969).

Figure 2. Ribbon diagram of the rabbit skeletal actin monomer structure as determined by Kabsch *et al.* (1990). This crystal structure was solved as a complex with DNase I. The structure shows actin to consist of two similar domains each of which contains a 5-stranded β-sheet and associated α-helices. ADP molecule and Ca ion (hatched circle) are located in the base of the cleft formed by the two domains. The two domains of roughly equivalent size are further divided to give the existence of discrete four subdomains.

Figure 3. An atomic model of filamentous actin (F-actin) proposed by Holmes *et al.* (1990). Using the atomic structure of the monomer (Figure2; Kabsch *et al.*, 1990) a model of the F-actin has been obtained by fitting the data to the observed X-ray diffraction pattern of oriented F-actin. In this model, F-actin has 13 actin molecules arranged on six left-handed turns repeating every 36 nm. The rise per subunit is 2.75 nm. The

morphology of the actin helix is two intertwined, long-pitch, right-handed helices. Along each of the morphological helices, the actin monomers are spaced by 5.5 nm.

Figure 4. (A) Two-step binding of myosin (or myosin-nucleotide complex) to actin (Geeves, 1991). M is myosin or a myosin subfragment, N is nucleotide and A is actin in this scheme. Kinetically the docking of myosin onto an actin filament can be resolved into at least two events. The essential proposals of this model are that the docking process is an inherent property of the acto-S1 proteins, that the role of ATP binding and hydrolysis is to allow this docking to be repeated, and that the last event in the docking (the A-to-R isomerization) is coupled to the fast product release from myosin active site (and so acceleration of myosin S1 ATPase) and the force generating event in muscle contraction. (B) The three-state model of thin filament regulation (McKillop & Geeves, 1993). A diagrammatic representation of the proposed three states of the thin filament is shown. The small filled circle represents tropomyosin, which can bind to three places on the actin surface covering different proportions of two myosin binding sites (triangular segments). The regulation of actin-myosin interaction in solution can be modeled adequately if the thin filament exists as a dynamic equilibrium between three calcium- and myosin-dependent states: blocked, closed and open. In the blocked state all binding is prevented; in the closed state the myosin S1 can bind to form the A-state but not the R-state; in the open state there is no inhibition, and the myosin can bind to form the A-state and isomerize to the R-state. In the absence of calcium the blocked state predominates with ~80 % of the actins in the filament in this form (20 % closed, <5 % open). In the presence of calcium but the absence of myosin heads the closed state predominates (<5 % blocked, 80 % closed, 20 % open). This is also the preferred state of troponin-free thin filaments. The transition from the closed state to the open state is induced by strongly bound myosin heads. Thus, the full activation of thin filaments requires not only calcium but also myosin heads.

Figure 5. Design of the mutant actins (Saeki *et al.*, 1996; Saeki & Wakabayashi, 2000).

Dictyostelium expression system was used to prepare mutant actins. Mutations were introduced into *Dictyostelium* actin 15 gene. In all mutants, Glu360 was changed to histidine to facilitate separation of mutant actins from the wild-type actin by DEAE column. The E360H mutant shows normal calcium regulation (Saeki *et al.*, 1996). The sequence of residues 228-232 (KAYKE) of the full chimera comes from *Tetrahymena* actin sequence. The *Tetrahymena* actin does not bind tropomyosin (Hirono *et al.*, 1990). The residues 228-232 on actin's subdomain 4 are the most divergent region between *Tetrahymena* actin and skeletal actin, except for N-terminus region where identity is generally low among species.

Figure 6. Activation of myosin S1 ATPase activities by various actins under three conditions, i. e., pure actin (hatched bars), in the presence of tropomyosin-troponin either with (black bars) or without calcium (dotted bars). Without tropomyosin-troponin all of the three mutants activated myosin S1 ATPase as the wild-type and this activation was suppressed by rabbit skeletal tropomyosion-troponin in the absence of Ca^{2+}. This indicates that the basic process of actin activation and the inhibitory process in mutant actin systems are indistinguishable from that of the wild-type one. However, the mutants showed higher ATPase activation than wild-type actin in the presence of tropomyosin-troponin and Ca^{2+}, i. e., they show "higher Ca^{2+}-activation." This indicates that only the Ca^{2+}-activation process is affected by these mutants. Note that only the point mutation A230Y causes this effect. The error bars represent standard deviations based on four measurements. Adapted from Saeki & Wakabayashi (2000).

Figure 7. (A) An orthorhombic crystal of a mutant actin (half chimera-1)-G1 complex. Typical largest dimension was about 1 mm. (B) A 3.0° oscillation photograph of a crystal of a mutant actin (half chimera-1)-G1 complex taken at SPring-8 beamline BL41XU. The rotation axis was horizontal. The boxed area is enlarged in the lower right corner with softer contrast to show the diffraction spots at high resolution. Diffraction spots were observed up to 1.7 Å resolution.

Figure 8. Overview of the crystal structure of the complex formed between wild-type *Dictyostelium* actin (yellow) and gelsolin segment 1 (light green). The ATP is shown as a ball-and-stick model and the calcium ions as orange spheres.

Figure 9. Crystal contact sites. The Cα atoms of the residues involved in crystal contacts are shown as black spheres.

Figure 10. Packing of actin-G1 complexes in an orthorhombic unit cell. There is one molecule in the asymmetric unit. There are four molecules (shown in different colours) in one unit cell.

Figure 11. An overview of crystal contacts. One molecule in this crystal makes contact with six neighbour molecules. In this view, contact sites 1 and 2 (Table 4) are clearly visible. These contacts are mediated by actin residues.

Figure 12. Another overview of crystal contacts. The yellow molecule and the two molecules (cyan and dark green) in the lowest part of Figure 11 are shown in the same colour as in Figure 11 and are viewed from the right side of Figure 11. The other molecules in Figure 11 are omitted from this figure for clarity. In this view, contact sites 3, 4 and 5 (Table 4) are clearly visible. The site 3 is the contact between G1 residues. The sites 4 and 5 are actin-G1 contact sites.

Figure 13. Stereo view of part of the final 2*Fo*–*Fc* map of (A) *Dictyostelium* wild-type actin, (B) half chimera-1 and (C) full chimera showing area near the mutation site (Q228K/T229A/A230Y or Q228K/T229A/A230Y/A231K/S232E) in subdomain 4. Figures 13, 16 and 17 were prepared using O (Jones *et al.*, 1991).

Figure 14. Superpositon of the main-chains for the three actins: *Dictyostelium* wild-type

(red), half chimera-1 (blue) and full chimera (green). The overall main-chain conformation is very similar for the three structures.

Figure 15. Plots of r.m.s. deviations for the main chain (red line graph) and side chain (blue bar chart): (A) comparison between *Dictyostelium* wild-type actin and half chimera-1, (B) comparison between *Dictyostelium* wild-type actin and full chimera, (C) comparison between half chimera-1 and full chimera. After the alignment of main chains with the program LSQKAB (CCP4, 1994; Kabsch, 1976), the r.m.s. deviations for each residue were calculated with the program DIFRES (CCP4, 1994).

Figure 16. 2*Fo*–*Fc* map around Glu100. Glu100 may take multiple conformations in the three structures.

Figure 17. 2*Fo*–*Fc* map around Gln354. Gln354 may take multiple conformations in the three structures.

Figure 18. Detail of the area surrounding the residues 228-232 in (A) *Dictyostelium* wild-type actin, (B) half chimera-1 and (C) full chimera. Mutated residues in (B) and (C) are shown in pink. Both chimera actin structures are similar in that the A230Y mutation causes the nonpolar side chain of Leu236 to be displaced from a hydrophobic pocket in the wild-type actin structure to a more exposed position in the mutant structure. This displacement produces a more extensive hydrophobic patch on the actin surface that may modulate the interaction between actin and tropomyosin-troponin with Ca^{2+}. This structural change correlates with ATPase data which indicates that only the A230Y mutation produces higher Ca^{2+}-activation in the presence of tropomyosin-troponin (Saeki & Wakabayashi, 2000).

Figure 19. CPK surfaces of (A) *Dictyostelium* wild-type actin, (B) half chimera-1 and (C) full chimera. The side chains of residue 230 (Ala in wild-type and Tyr in the

mutants) and Leu236 are shown in red and green, respectively. The A230Y mutation significantly increases the solvent accessibility of Leu236.

Figure 20. Schematic representation showing the interaction between Ca^{2+}ATP and a mutant actin (half chimera-1). Water molecules (pink spheres) are important for mediating both the interaction between the adenine ring and actin and also for the binding of the Ca^{2+} and phosphate. The adenine base fits in a hydrophobic pocket (yellow thick line) but many of its hydrogen-bonded interactions with polar groups on actin are mediated through water molecules. Similarly, the interactions of Ca^{2+} to acidic residues on actin such as aspartates 11 and 154 are mediated through water molecules. Dashed cyan lines correspond to hydrogen bonds or electrostatic interactions. The corresponding distances in Å are given next to the dashed lines. The distance in Å between Wat203 and the γ-phosphorous is also given next to a black arrow.

Figure 21. Stereo view illustrating the interactions around the ATP γ-phosphate in half chimera-1. Ca^{2+} ion and water molecules are depicted in yellow and pink, respectively. Dotted cyan lines represent hydrogen bonds. Wat203 is located approximately in-line to the β–γ bond.

Figure 22. Three-dimensional reconstruction of thin filaments fully decorated with myosin S1 in the absence of ATP (Vibert *et al.*, 1997). This probably corresponds to the "open-state" in the three-state model (see Figure 4). Tropomyosin density is indicated by arrows and the zones of actin residues reported to interact with myosin (Rayment *et al.*, 1993) are highlighted in red. The Cα position of residue 230 is shown as a white sphere in the actin monomer Cα-backbone model (Lorenz *et al.*, 1993). The region around residue 230 probably forms part of tropomyosin binding sites in the "open-state."

Figure 23. Amino acid sequence of α-tropomyosin drawn in (19 + 2/3) - residue repeat pattern with 14 bands in first 275-residues (McLachlan & Stewart, 1976). Some amino

acids appear twice for clarity. Negative charges are ringed (○) and concentrated in the negative zone. Non-polar groups in positions *b, c, f* are marked (◇) and lie in the hydrophobic zone. (•) Marks end of 7-residue heptapeptides. Boxes show: (i) residues 1 to 9 and 276 to 284, which are believed to overlap in head-to-tail linkage; (ii) anomalous regions near Cys190 between residues 197 and 217 which lack acid groups in negative zones and may form troponin binding site. To maintain continuity, the amino acids that lie near the left and right-hand margins of each row are drawn twice.

Figure 24. Comparison of actin amino acid sequences between rabbit (Collins & Elzinga, 1975), *Dictyostelium* (Vandekerckhove & Weber, 1980; Romans & Firtel, 1985) and *Tetrahymena* (Hirono *et al.*, 1987). Conserved residues are shown in black boxes.

Figure 25. Three-dimensional positions of the non-conserved actin residues in Figure 24 which may relate to the functional differences between rabbit, *Dictyostelium* and *Tetrahymena* actins. Completely non-conserved residues (i. e., all three actins have different residues in these positions) are shown in yellow. Residues conserved between rabbit and *Dictyostelium* but not in *Tatrahymena* are shown in red. Residues conserved between *Dictyostelium* and *Tetrahymena* but not in rabbit are shown in purple.

Tables and Figures

Table 1. Fractional occupancy of the three states of thin filaments (Schaertl *et al.*, 1995)

Thin filaments	blocked	closed	open
actin			1.0
actin/Tm		0.8	0.2
actin/Tm/Tn + Ca^{2+}		0.8	0.2
actin/Tm/Tn – Ca^{2+}	0.7	0.25	0.05
any filament + S1[a]			1.0

[a] Strongly bound R-type complexes.

Table 2. Data collection statistics

	Dicty wild-type	half chimera-1	full chimera
Space group	$P2_12_12_1$	$P2_12_12_1$	$P2_12_12_1$
Unit cell (Å)			
	$a = 57.0$	$a = 56.9$	$a = 56.9$
	$b = 69.6$	$b = 69.0$	$b = 69.4$
	$c = 184.6$	$c = 181.5$	$c = 183.2$
Resolution range (Å) [a]	29.1-2.4 (2.52-2.4)	30.0-2.0 (2.11-2.0)	30.0-2.4 (2.49-2.4)
Total observations	68,469	161,420	96,715
Unique reflections	27,962	45,284	27,352
Completeness (%)	94.9	92.6	93.5
R_{merge} (%) [ab]	7.4 (15.5)	6.4 (14.9)	3.3 (5.5)
I/σ [a]	8.0 (4.5)	8.0 (4.6)	29.6 (19.3)

[a] Parentheses refer to final resolution shell.

[b] $R_{merge} = \Sigma_{hkl}\Sigma_i \, |I(hkl)_i - \langle I(hkl)\rangle| \, / \, \Sigma_{hkl}\Sigma_i \, |I(hkl)_i|$, where $\langle I(hkl)\rangle$ is the mean intensity of equivalent reflections

Table 3. Refinement statistics

	Dicty wild-type	half chimera-1	full chimera
Resolution range (Å)	10.0-2.4	10.0-2.0	10.0-2.4
Number of non-H atoms			
protein	3856	3862	3869
ATP	31	31	31
Ca^{2+}	3	3	3
water	394	469	405
R-factor (%) [a]	18.3	18.2	17.1
Free *R*-factor (%) [b]	23.1	22.3	21.4
Bond length r.m.s. (Å)	0.010	0.011	0.013
Bond angle r.m.s. (deg.)	1.9	1.9	1.9
Ramachandran plot			
Most favoured (%)	93.4	94.5	93.8
Allowed (%)	6.6	5.5	6.2
Generously allowed (%)	0	0	0
Forbidden (%)	0	0	0

[a] $R = \Sigma\ |Fo-Fc| / \Sigma\ |Fo|$, where *Fo* and *Fc* are the observed and calculated structure factor amplitudes, respectively.

[b] Free $R = \Sigma\ |Fo-Fc| / \Sigma\ |Fo|$, computed using 5 % of the data assigned randomly.

Table 4. Residues involved in crystal contacts in the orthorhombic crystal of actin-G1 complex

	Residue numbers (residues in one molecule --- contacted residues in a neighbor molecule)
site 1	actin 95 --- actin 323
site 2	actin 60, 63 --- actin 195, 196
site 3	G1 69 --- G1 88, 91
site 4	actin 333, 334 --- G1 56, 57
site 5	actin 169, 372, 375 --- G1 118, 120

Table 5. Solvent accessibility of Leu236

Structures	Solvent accessible surface area of the side chain of Leu236 ($Å^2$) [a]	References	PDB accession code
Dictyostelium full chimera mutant actin: gelsolin segment 1	27.1	This paper	1DEJ
Dictyostellium half chimera-1 mutant actin: gelsolin segment 1	19.6	This paper	1C0G
Dictyostelium wild-type actin: gelsolin segment 1	6.5	This paper	1C0F
Rabbit skeletal α-actin: gelsolin segment 1	9.0	McLaughlin *et al.* (1993)	Provided by Mr. B. Pope
Rabbit skeletal α-actin: DNase I	5.6	Kabsch *et al.* (1990)	1ATN
β-actin: profilin (tight state)	11.2	Schutt *et al.* (1993)	2BTF
β-actin: profilin (open state)	7.5	Chik *et al.* (1996)	1HLU

[a] Calculated with the program SURFACE (CCP4, 1994). Standard van der Waals radii and a probe radius of 1.4 Å were used in the computation.

Table 6. The overall affinity of tropomyosin to various actins as determined by co-sedimentation (Saeki & Wakabayashi, 2000)

actin	sequence of residues 228-232	actin-tropomyosin binding K_{app} (μM)
Dicty wild-type	QTAAS	0.95 ± 0.09
A230Y	QT**Y**AS	1.13 ± 0.12
half chimera-1	**KAY**AS	1.03 ± 0.17
full chimera	**KAYKE**	1.65 ± 0.17

Table 7. Percentage homologies between actin amino acid sequences

	rabbit skeletal	*Dictyostelium*
Dictyostelium	91.2	
Tetrahymena	74.6	76.3

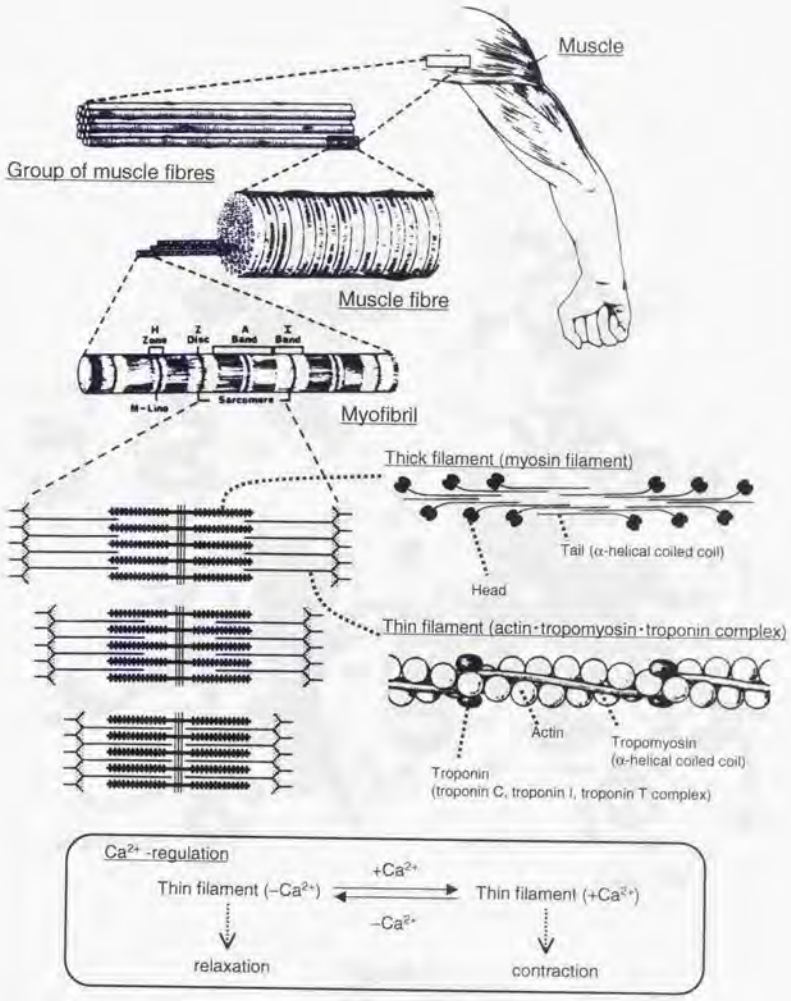
Muscle
Group of muscle fibres
Muscle fibre
H Zone
Z Disc
A Band
I Band
M-Line
Sarcomere
Myofibril
Thick filament (myosin filament)
Tail (α-helical coiled coil)
Head
Thin filament (actin·tropomyosin·troponin complex)
Actin
Tropomyosin (α-helical coiled coil)
Troponin (troponin C, troponin I, troponin T complex)
Ca2+ -regulation
Thin filament (–Ca2+)
+Ca2+
–Ca2+
Thin filament (+Ca2+)
relaxation
contraction

Figure 1

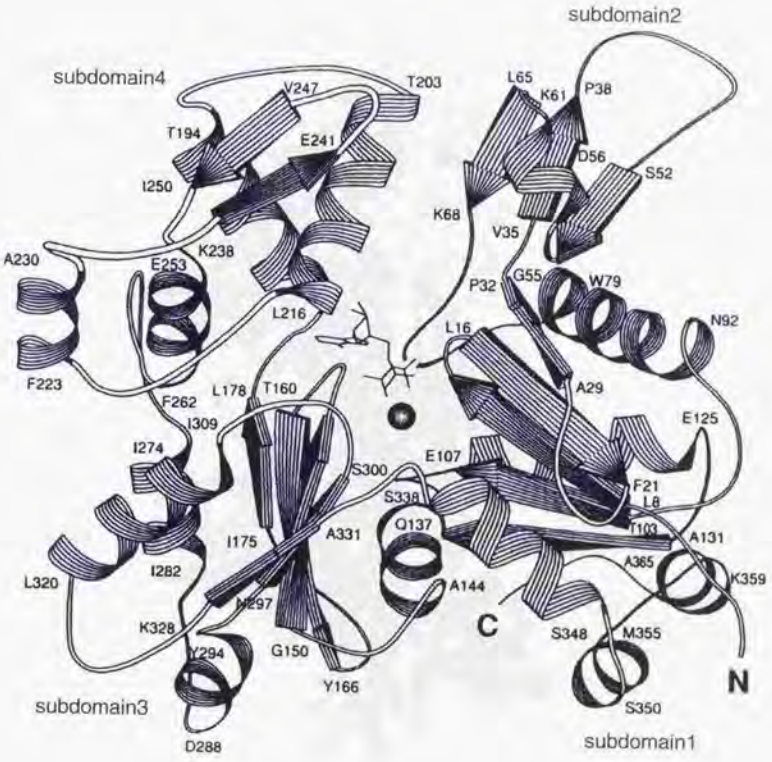
subdomain2
subdomain4
V247
T203
L65
K61
P38
T194
E241
D56
S52
I250
K68
V35
A230
K238
E253
P32
G55
W79
L216
L16
N92
F223
L178
T160
A29
F262
I309
E125
I274
E107
S300
F21
S336
L8
Q137
T100
A131
I175
A331
A365
K359
L320
I282
A144
M297
C
K328
S348
M355
G150
Y294
Y166
N
S350
subdomain3
subdomain1
D288

Figure 2

(pointed end)

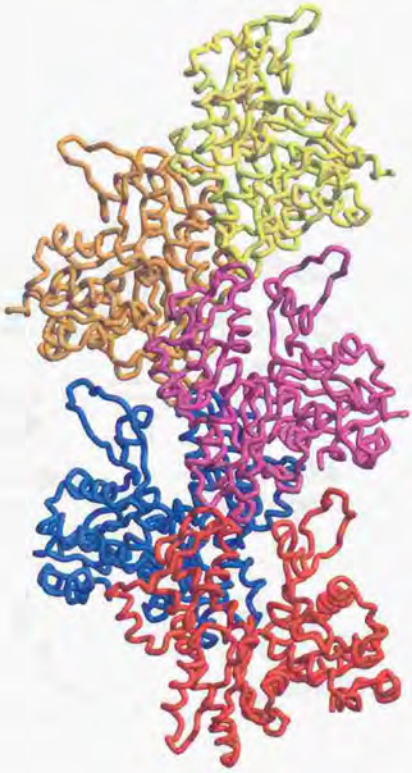

(barbed end)

Figure 3

(A) two-step binding of myosin to actin

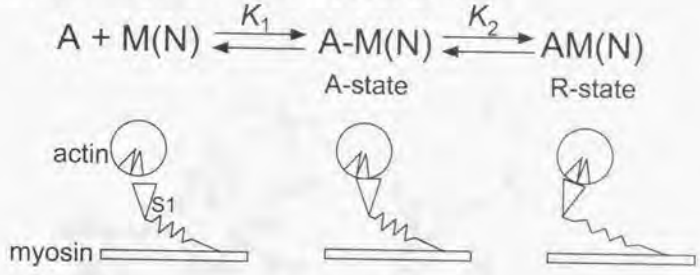

(B) three-state model of Ca^{2+}-regulation

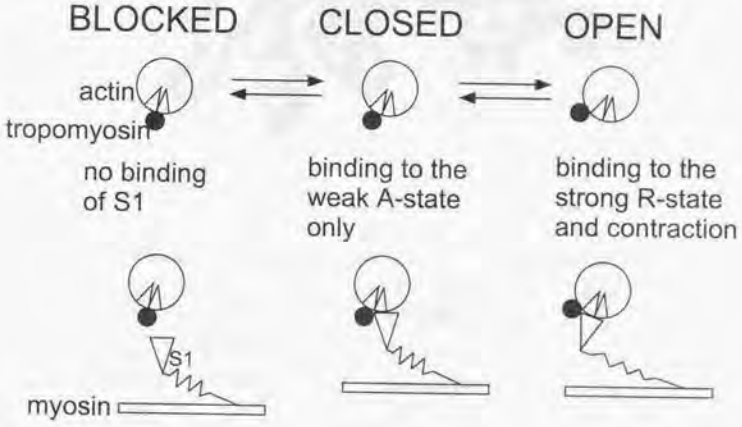

Figure 4

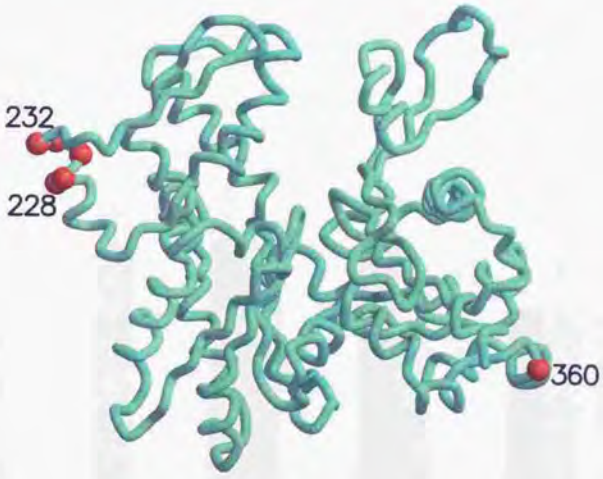

	228 232	360
Dicty wild	QTAAS ------	E
full chimera	KAYKE ------	H
half chimera-1	KAYAS ------	H
A230Y	QTYAS ------	H

Figure 5

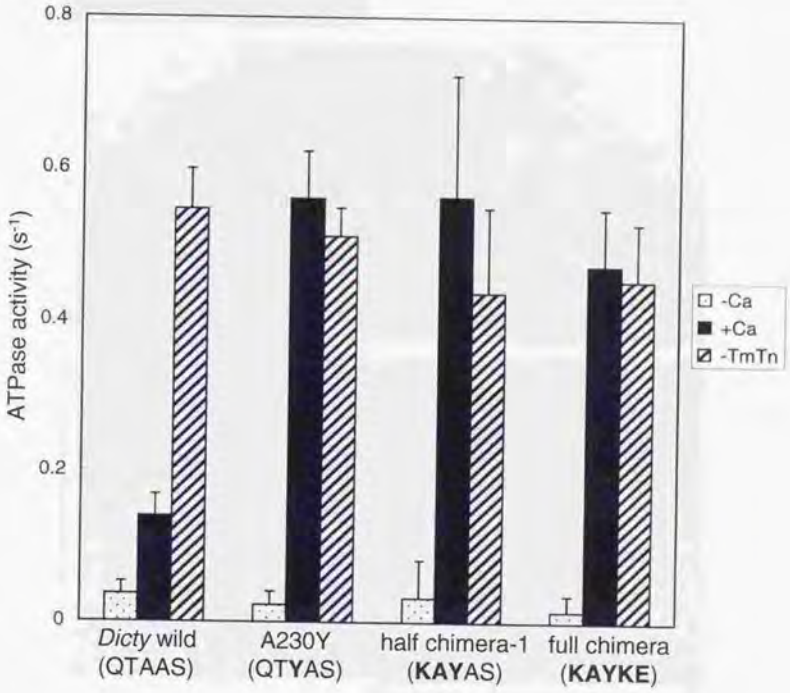
0.8
0.6
0.4
0.2
0
ATPase activity (s^{-1})
-Ca
+Ca
-TmTn
Dicty wild (QTAAS)
A230Y (QTYAS)
half chimera-1 (**KAY**AS)
full chimera (**KAYKE**)

Figure 6

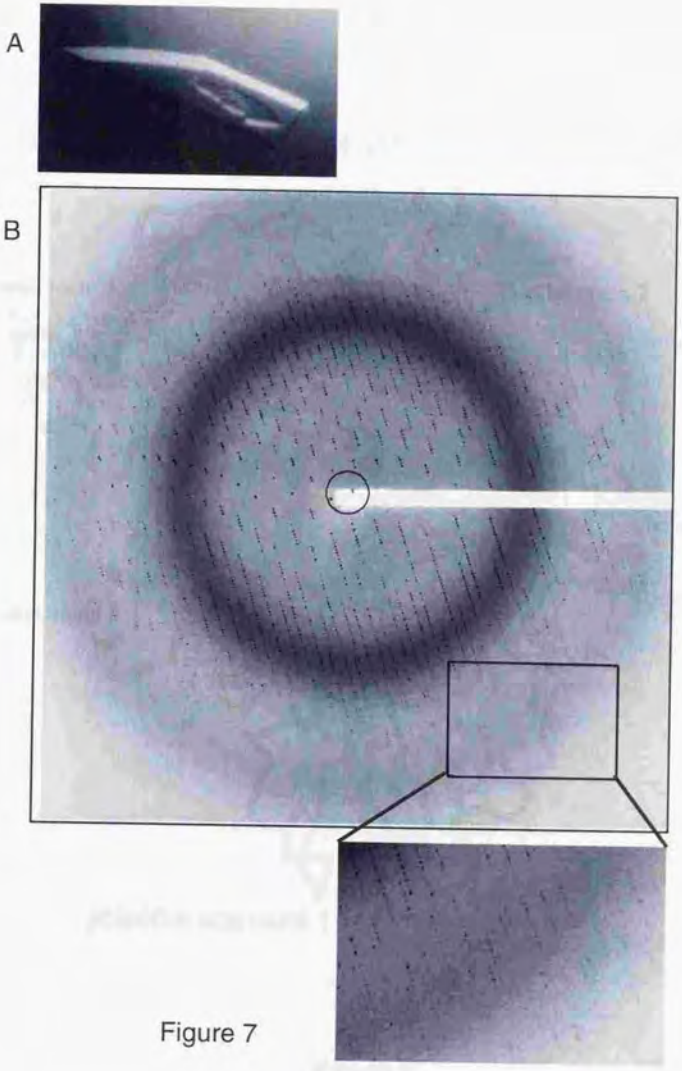

Figure 7

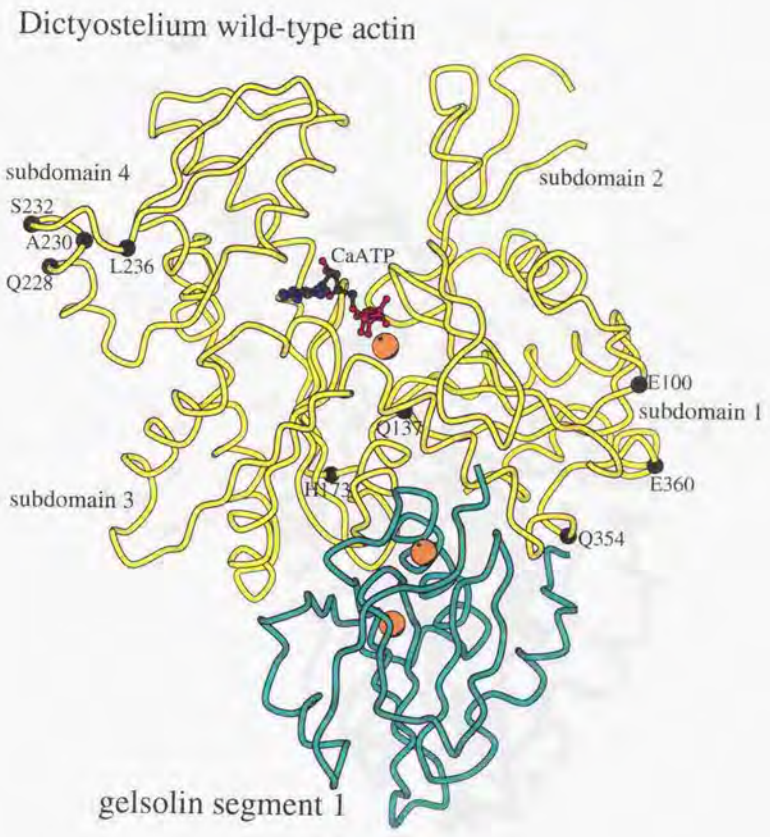
Dictyostelium wild-type actin
subdomain 4
S232
A230
Q228
L236
CaATP
subdomain 2
E100
subdomain 1
Q137
H173
subdomain 3
E360
Q354
gelsolin segment 1

Figure 8

Residues involved in crystal contacts

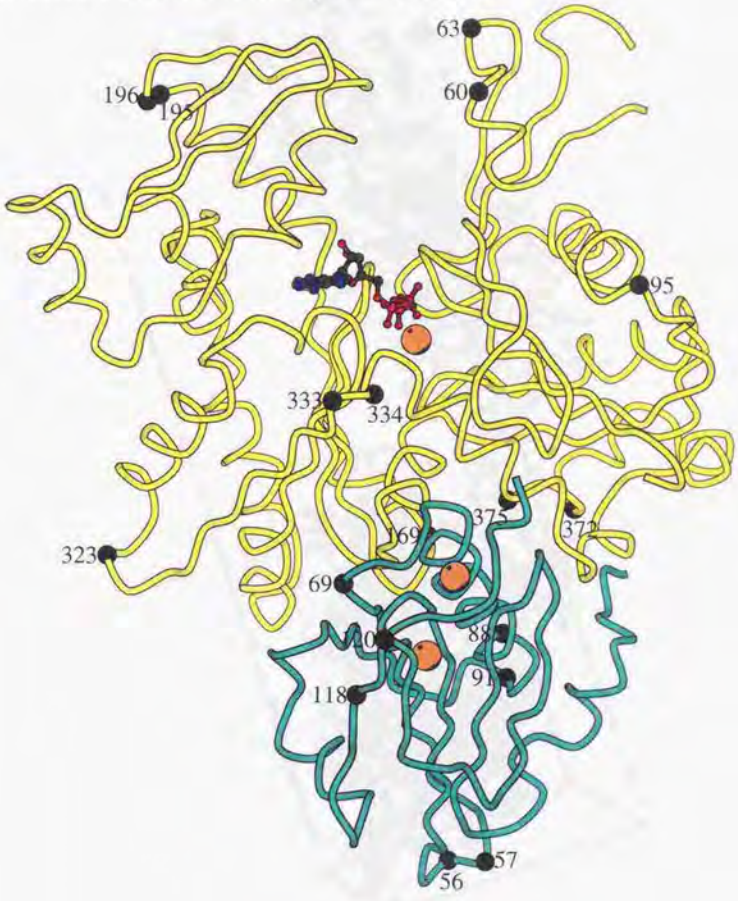

Figure 9

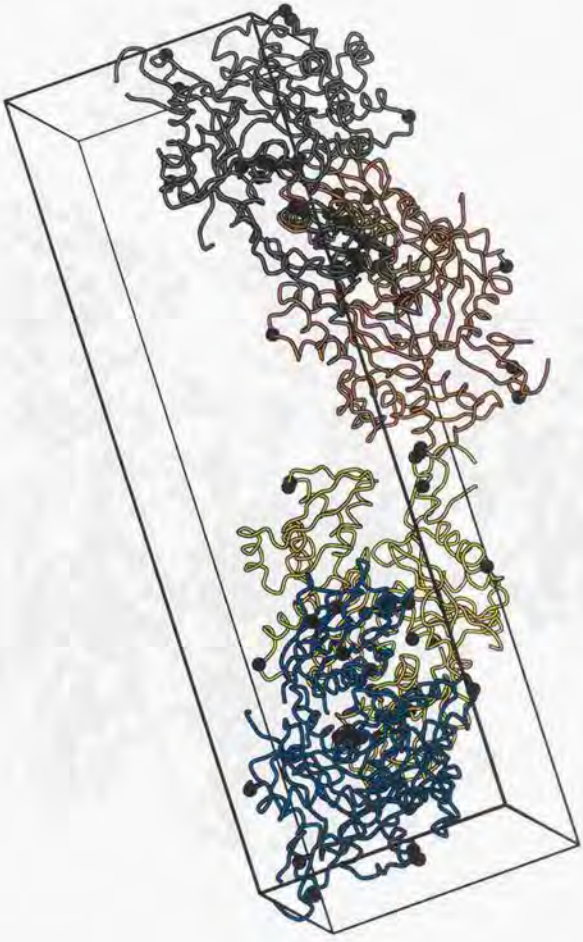

Figure 10

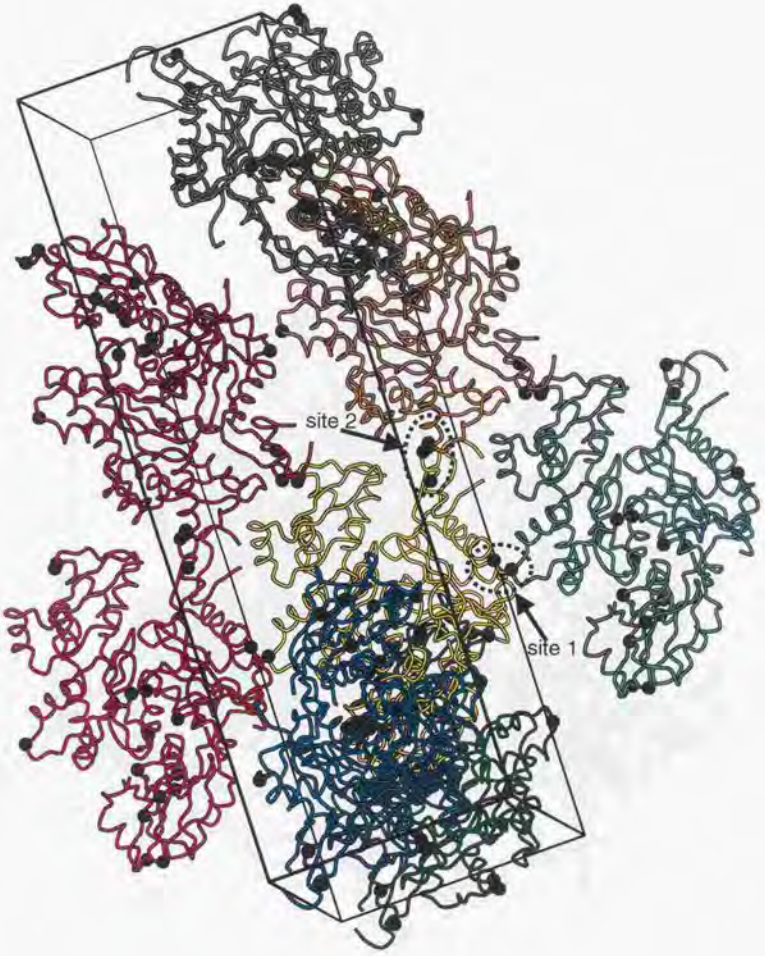

Figure 11

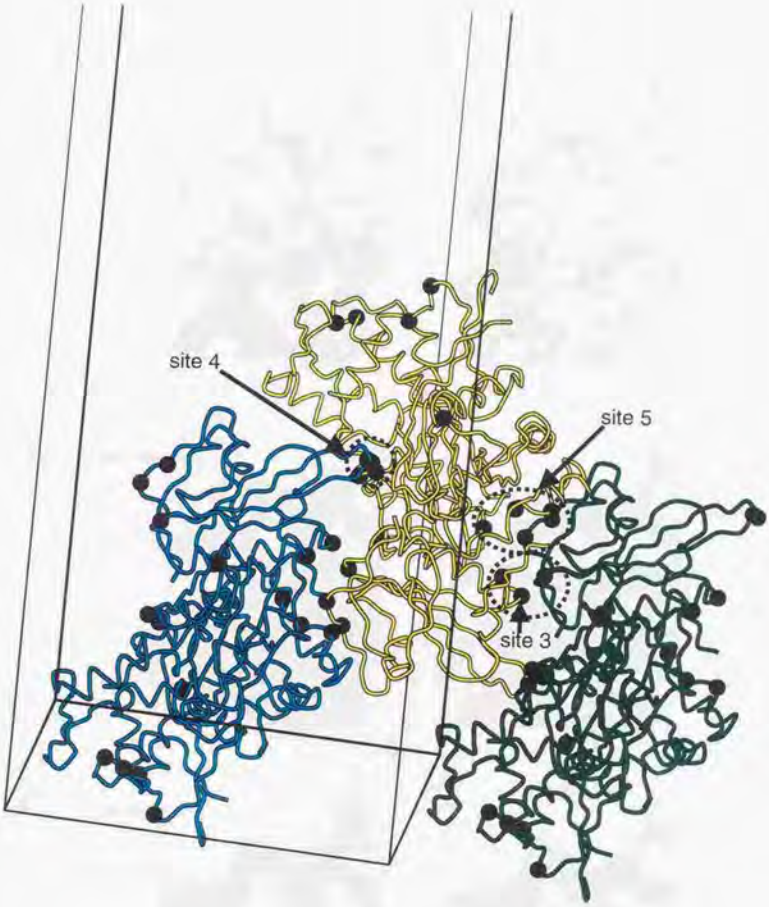

Figure 12

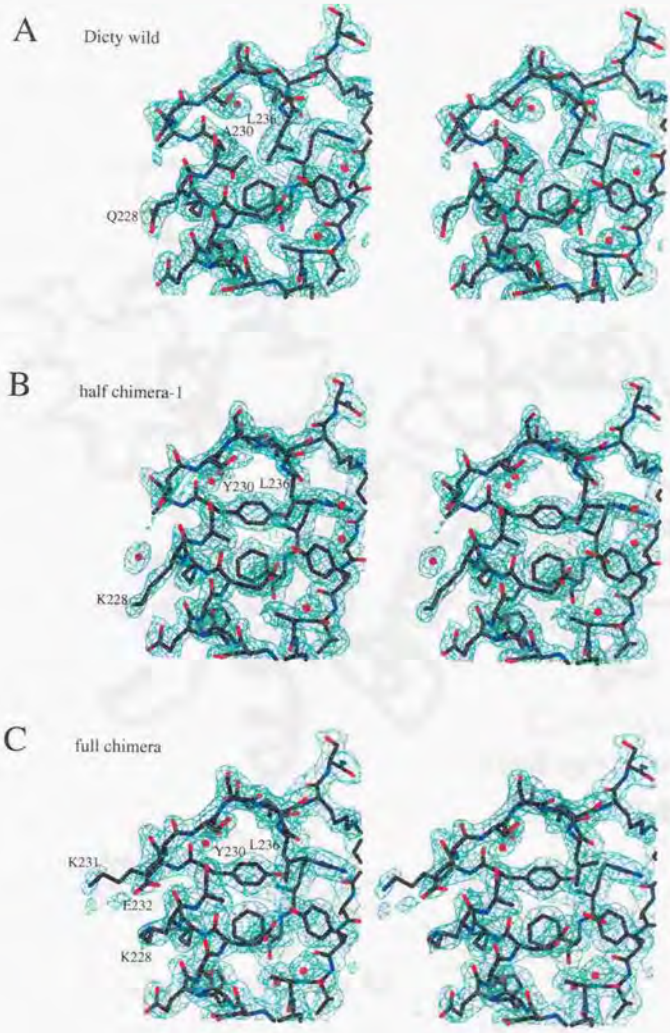
A
Dicty wild
L236
A230
Q228
B
half chimera-1
Y230
L236
K228
C
full chimera
K231
Y230
L236
E232
K228

Figure 13

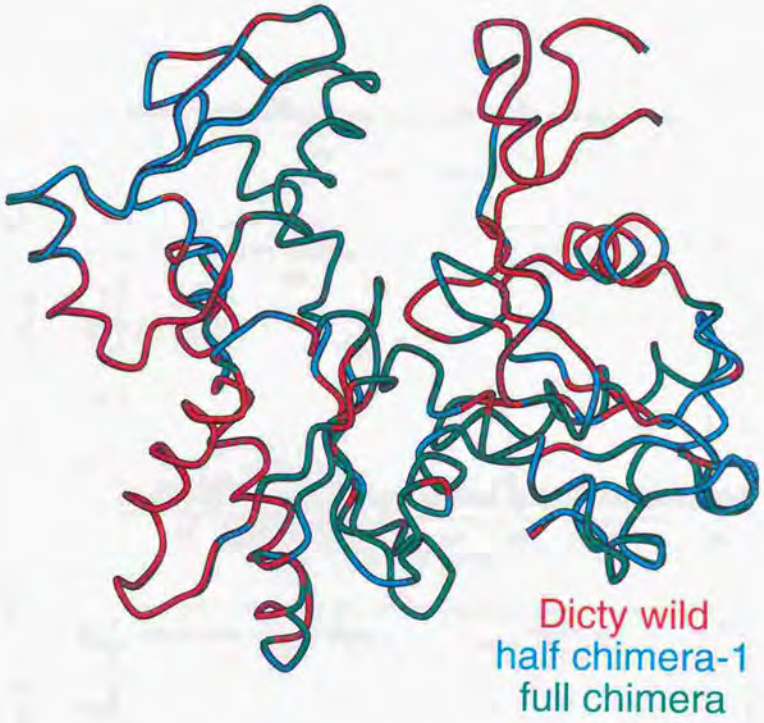

Figure 14

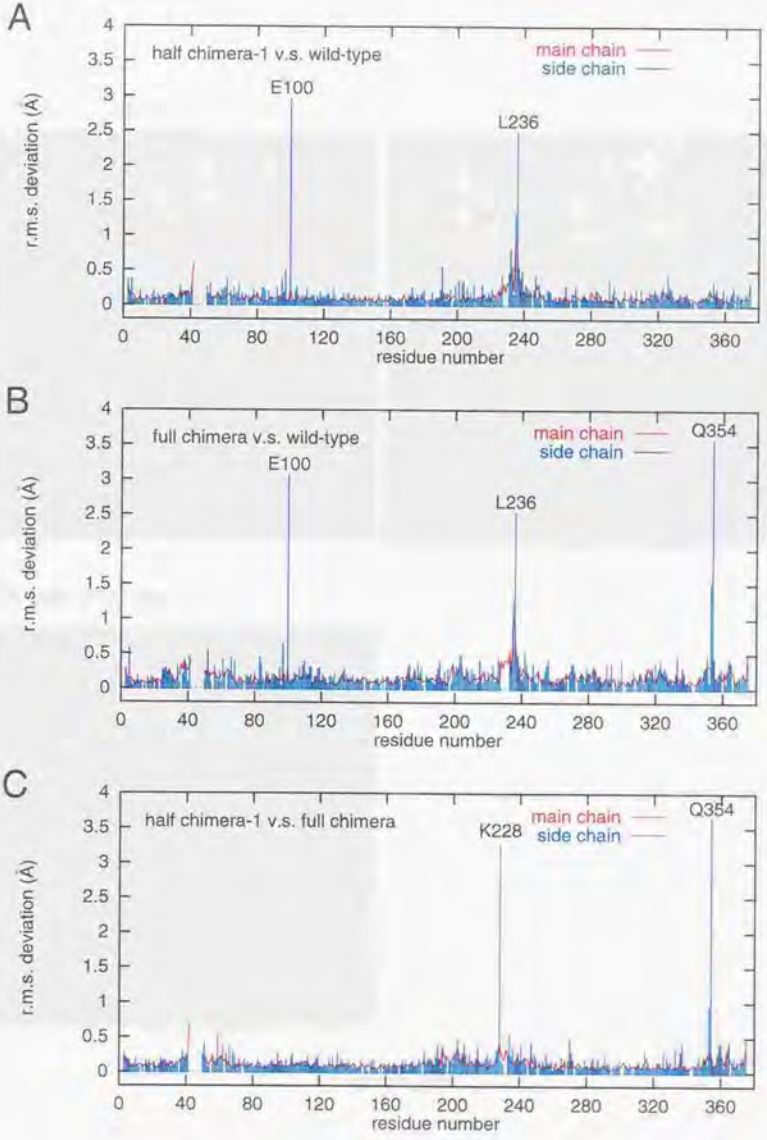
A
half chimera-1 v.s. wild-type
main chain
side chain
E100
L236
r.m.s. deviation (Å)
residue number
B
full chimera v.s. wild-type
main chain
side chain
E100
L236
Q354
r.m.s. deviation (Å)
residue number
C
half chimera-1 v.s. full chimera
main chain
side chain
K228
Q354
r.m.s. deviation (Å)
residue number

Figure 15

(A) *Dicty* wild

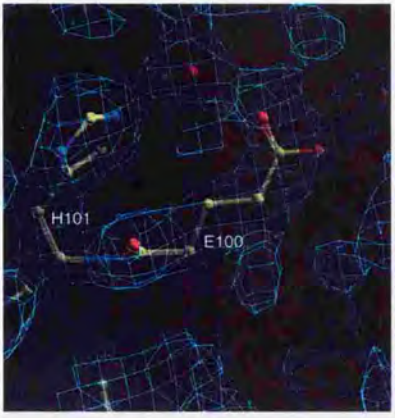

(C) full chimera

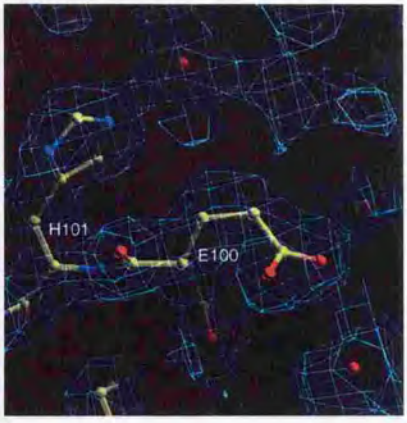

(B) half chimera-1

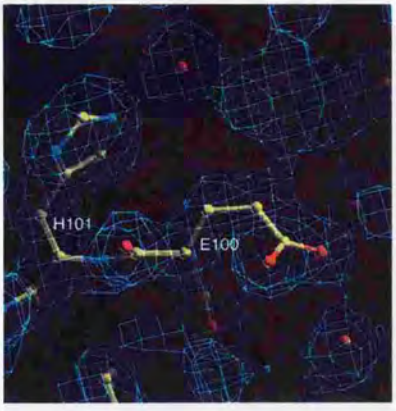

Figure 16

(A) *Dicty* wild

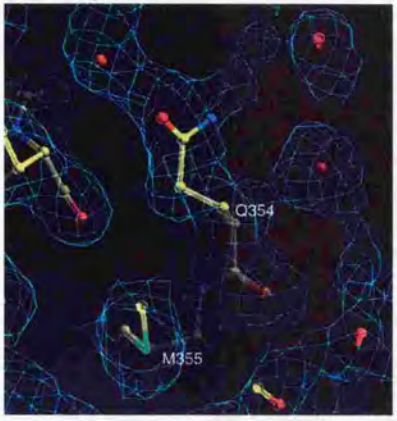

(C) full chimera

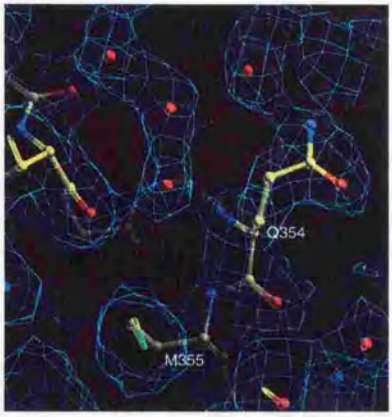

(B) half chimera-1

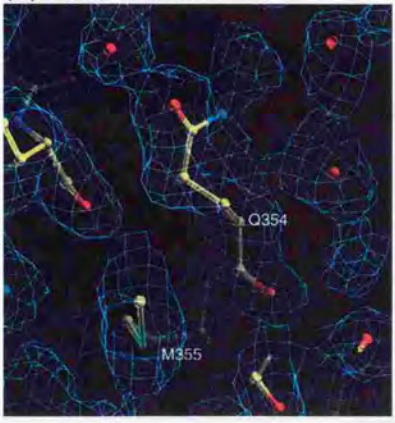

Figure 17

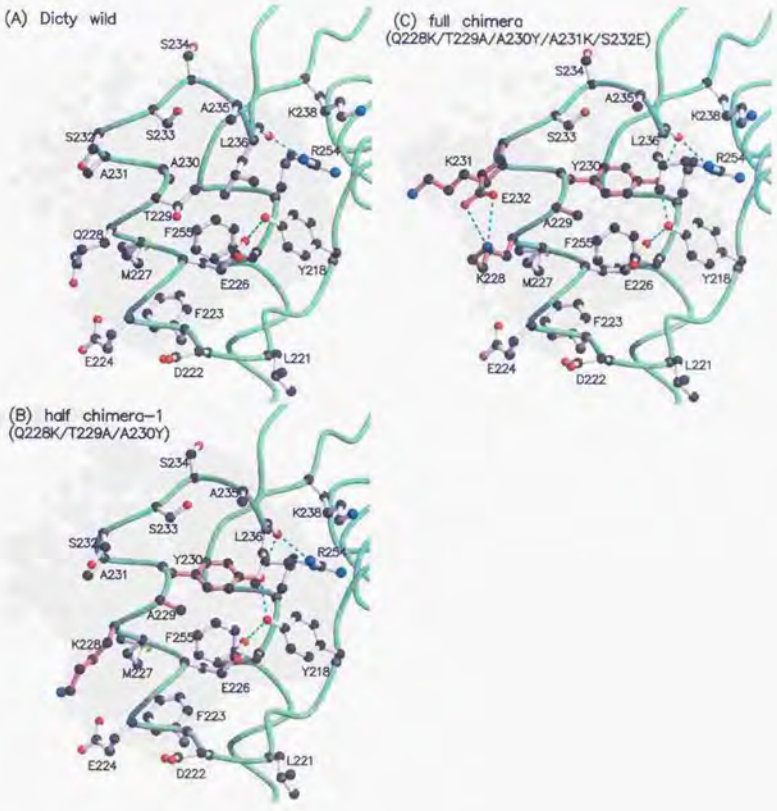
(A) Dicty wild
S234
A235
K238
S232
S233
L236
R254
A231
A230
T229
Q228
F255
M227
E226
Y218
F223
E224
D222
L221
(C) full chimera
(Q228K/T229A/A230Y/A231K/S232E)
S234
A235
K238
S233
L236
R254
K231
Y230
E232
A229
F255
K228
M227
E226
Y218
F223
E224
D222
L221
(B) half chimera-1
(Q228K/T229A/A230Y)
S234
A235
K238
S233
S232
L236
R254
Y230
A231
A229
K228
F255
M227
E226
Y218
F223
E224
D222
L221

Figure 18

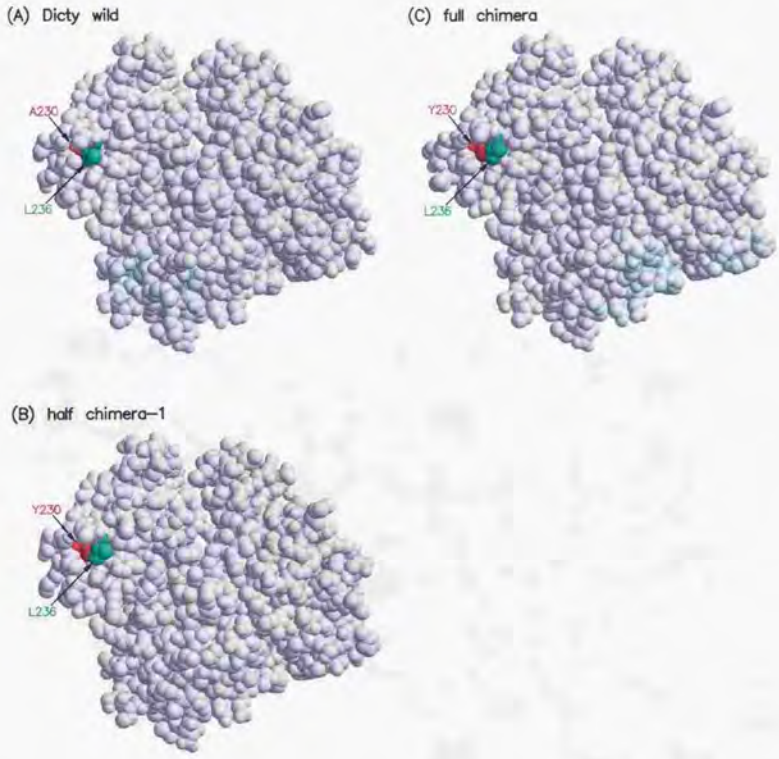
(A) Dicty wild
A230
L236
(C) full chimera
Y230
L236
(B) half chimera-1
Y230
L236

Figure 19

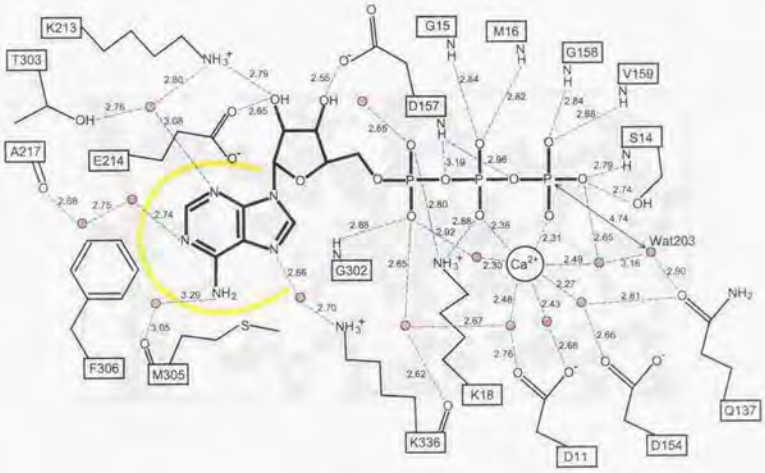
K213
T303
A217
E214
F306
M305
G302
D157
G15
M16
G158
V159
S14
Wat203
K18
K336
D11
D154
Q137
Ca2+

Figure 20

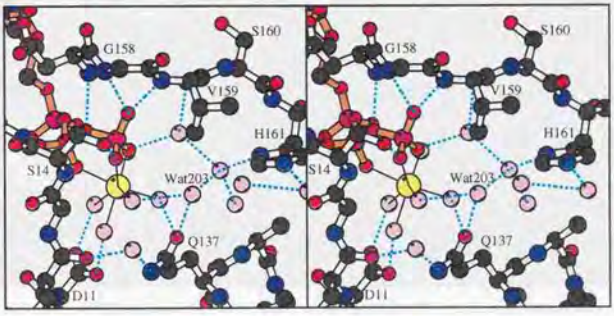
S160
G158
V159
H161
S14
Wat203
Q137
D11
S160
G158
V159
H161
S14
Wat203
Q137
D11

Figure 21

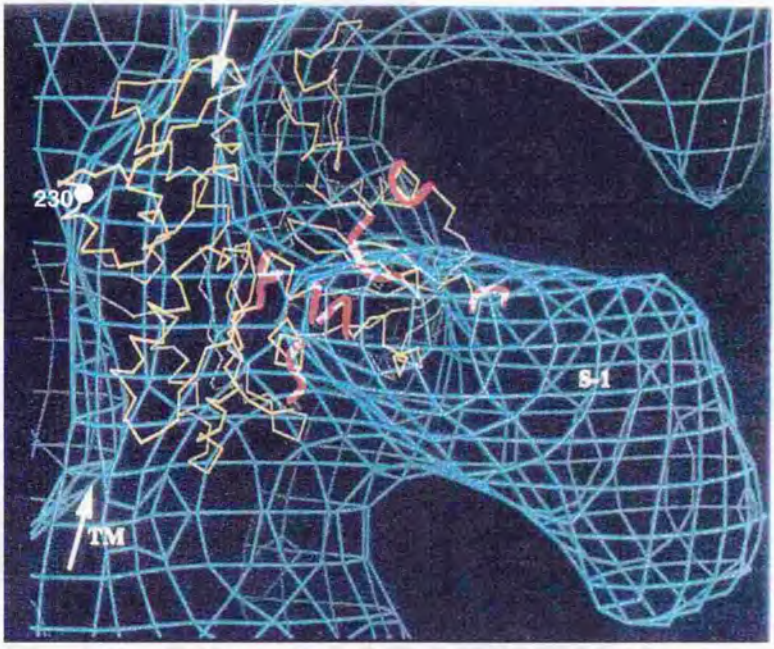

Figure 22

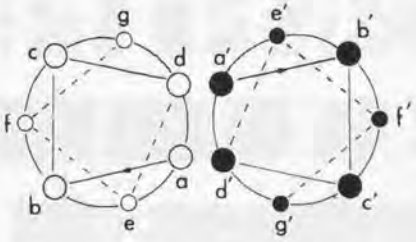
g
c
d
f
a
b
e
e′
b′
a′
f′
d′
c′
g′

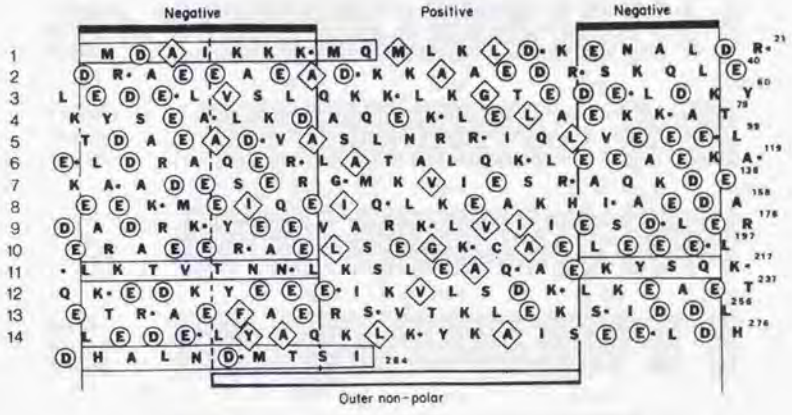
Negative
Positive
Negative
Outer non-polar

Figure 23

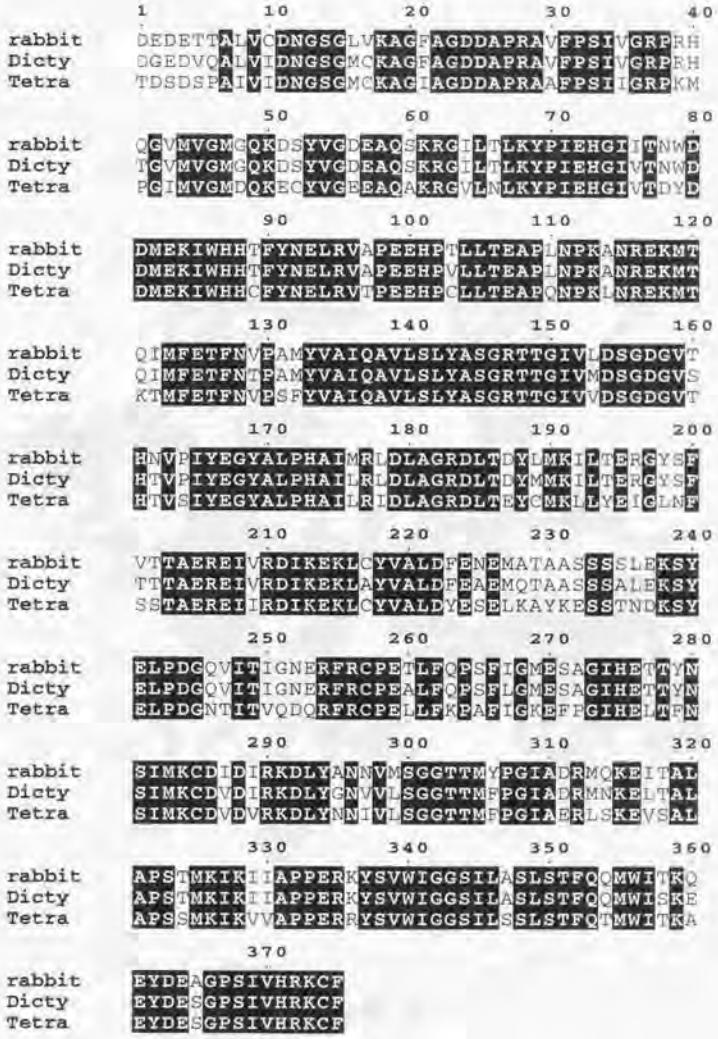
1 10 20 30 40
rabbit DEDETTALVCDNGSGLVKAGFAGDDAPRAVFPSIVGRPRH
Dicty DGEDVQALVIDNGSGMCKAGFAGDDAPRAVFPSIVGRPRH
Tetra TDSDSPAIVIDNGSGMCKAGIAGDDAPRAAFPSIIGRPKM
50 60 70 80
rabbit QGVMVGMGQKDSYVGDEAQSKRGILTLKYPIEHGIITNWD
Dicty TGVMVGMGQKDSYVGDEAQSKRGILTLKYPIEHGIVTNWD
Tetra PGIMVGMDQKECYVGDEAQAKRGVLNLKYPIEHGIVTDYD
90 100 110 120
rabbit DMEKIWHHTFYNELRVAPEEHPTLLTEAPLNPKANREKMT
Dicty DMEKIWHHTFYNELRVAPEEHPVLLTEAPLNPKANREKMT
Tetra DMEKIWHHCFYNELRVTPEEHPCLLTEAPQNPKLNREKMT
130 140 150 160
rabbit QIMFETFNVPAMYVAIQAVLSLYASGRTTGIVLDSGDGVT
Dicty QIMFETFNTPAMYVAIQAVLSLYASGRTTGIVMDSGDGVS
Tetra KTMFETFNVPSFYVAIQAVLSLYASGRTTGIVVDSGDGVT
170 180 190 200
rabbit HNVPIYEGYALPHAIMRLDLAGRDLTDYLMKILTERGYSF
Dicty HTVPIYEGYALPHAILRLDLAGRDLTDYMMKILTERGYSF
Tetra HTVSIYEGYALPHAILRIDLAGRDLTEYCMKLLYERGLNF
210 220 230 240
rabbit VTTAEREIVRDIKEKLCYVALDFENEMATAASSSSLEKSY
Dicty TTTAEREIVRDIKEKLAYVALDFEAEMQTAASSSALEKSY
Tetra SSTAEREIIRDIKEKLCYVALDYESELKAYKESSTNDKSY
250 260 270 280
rabbit ELPDGQVITIGNERFRCPETLFQPSFIGMESAGIHETTYN
Dicty ELPDGQVITIGNERFRCPEALFQPSFLGMESAGIHETTYN
Tetra ELPDGNTITVQDQRFRCPELLFKPAFIGKEFPGIHEITFN
290 300 310 320
rabbit SIMKCDIDIRKDLYANNVMSGGTTMYPGIADRMQKEITAL
Dicty SIMKCDVDIRKDLYGNVVLSGGTTMFPGIADRMNKELTAL
Tetra SIMKCDVDVRKDLYNNIVLSGGTTMFPGIAERLSKEVSAL
330 340 350 360
rabbit APSTMKIKIIAPPERKYSVWIGGSILASLSTFQQMWITKQ
Dicty APSTMKIKIIAPPERKYSVWIGGSILASLSTFQQMWISKE
Tetra APSSMKIKVVAPPERRYSVWIGGSILSSLSTFQTMWITKA
370
rabbit EYDEAGPSIVHRKCF
Dicty EYDESGPSIVHRKCF
Tetra EYDESGPSIVHRKCF

Figure 24

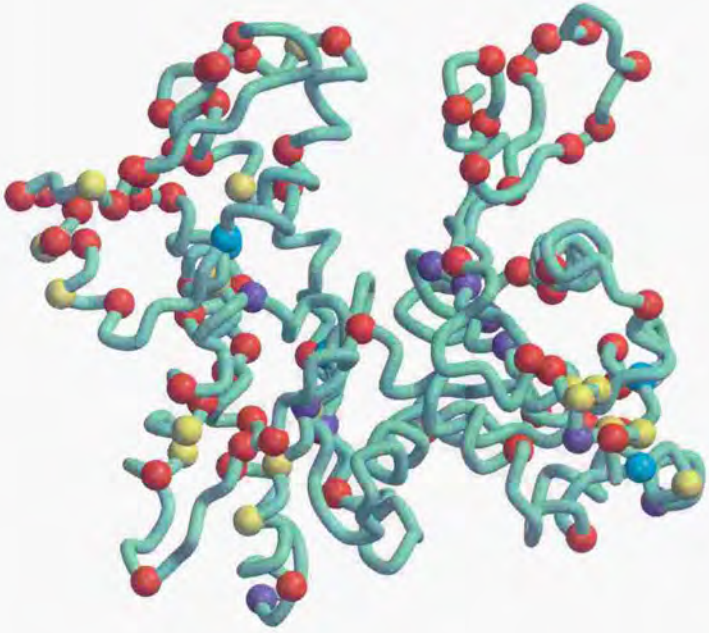

Figure 25

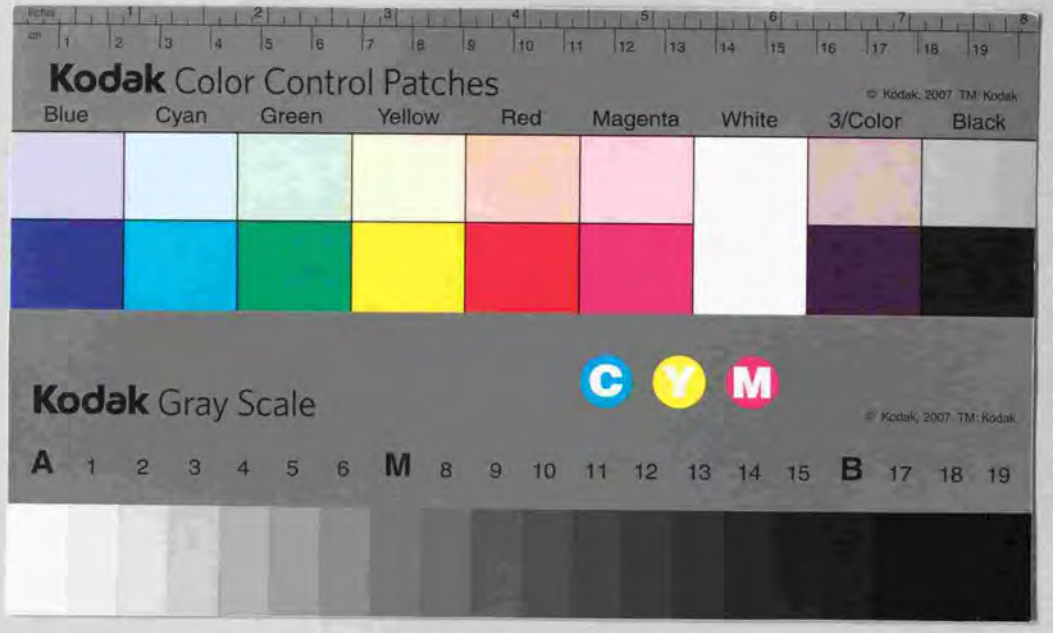
Kodak Color Control Patches
© Kodak, 2007 TM: Kodak
Blue
Cyan
Green
Yellow
Red
Magenta
White
3/Color
Black
Kodak Gray Scale
C
Y
M
© Kodak, 2007 TM: Kodak
A 1 2 3 4 5 6 M 8 9 10 11 12 13 14 15 B 17 18 19